A Finite Element Study of an Elastic- Plastic Axisymmetric Sinusoidal Surface Asperity in Contact Against a Rigid Flat with Strain Hardening

by

Geetanj Bhandari

A thesis submitted to the Graduate Faculty of
Auburn University
In partial fulfillment of the
requirements for the degree of
Master of Science

Auburn, Alabama
May 7, 2018

Keywords: Elastic-plastic, Finite Element Model, Hardening exponent

Approved by

Robert L. Jackson, Chair, Professor of Mechanical Engineering
Jeffery C. Suhling, Department Chair of Mechanical Engineering
Nima Shamsaei, Associate Professor of Mechanical Engineering

Abstract

With the advancement in science and the introduction of new technology, computational modelling of contact between rough surfaces has attracted a great deal of attention. Researchers have developed many rough surface contact models to simulate the elastic-plastic contact of spheres. Most of the early models of rough surface contacts assumed a cylindrical or spherical/ellipsoidal shape for the asperities on the surface, Sinusoidal models have also been introduced but not widely use until recently. However, at initial contact the spherical and sinusoidal cases are very similar and can both be described by the classic elastic Hertz contact case. However, there does not appear to exist a closed-form analytical model for elastic- plastic three dimensional sinusoidal contact. Elastic-plastic sinusoidal contact has recently become more important with the development of several multiscale contact models. This work uses a finite element model (FEM) to characterize elastic-plastic sinusoidal contact as it is pressed against a rigid surface. It is theorized that the sinusoidal asperity gives a better prediction of asperity interaction, especially for heavy loaded contacts. The current model is designed in such a way that it's axisymmetric and the interactions with the adjacent asperities are considered by the effect of periodicity at the base of the asperity. The material of the three dimensional axisymmetric sinusoidal surface is modelled as an elastic-plastic, nonlinear isotropic power law hardening solid. This work also characterizes the pressure required to cause complete contact between the surfaces. Complete contact is defined as when there is no gap between the two surfaces in contact. In the end, the FEM model is used to produce equations which can be employed to approximately relate

the area of contact to the contact pressure for elastic-plastic strain hardening sinusoidal contact. It was found that with the increase in hardening exponent and tangent modulus more pressure is required for complete contact to occur. The results are also curve fitted to provide an expression for the contact area over a wide range of cases for use in engineering applications.

Acknowledgments

First of all, I would like to offer my heartfelt salutation to the Supreme Being for the physical and mental strength bestowed upon me and in whose faith, I was able to complete this task. I am deeply indebted to my committee chair, Dr. Robert L. Jackson, who has the attitude and the substance of a genius. Without his technical, educational, and moral support this thesis would not have been possible. I should thank Prof. Jeffery C. Suhling and Prof. Nima Shamsaei for serving on my thesis committee. I also should thank my group mates Swarna Saha, Yang Xu, Alex Locker for their support and friendship.

For the ancestors who paved the path before me upon whose shoulders I stand. I owe this pride place to my Father- Surinder Jit Singh Bhandari and Mother- Sarla Bhandari. Their unwavering, ecstatic love, dedication and determination has always rejuvenated my strength and rekindled my sense of duty.

Above all, I would like to express my deepest gratitude to my loving Sisters- Sheetal Bhandari and Nishu Bhandari, and my nephews, Brothers-in-law and grandparents for their endless love and unflinching support during my whole life and without whom I would not have achieved my goals. Thank you for everything.

Table of Contents

List of Figures

<p style="text-align:center">List of Tables</p>

<p style="text-align:center">x</p>

List of Abbreviations

E	Elastic modulus
E_T	Tangential modulus
n	Hardening exponent
λ	Wavelength of sinusoidal surface
Δ	Amplitude of sinusoidal surface
ν_i	Poisson's ratio
E'	Equivalent elastic modulus
Δ_c	Critical interference
$\Phi(z)$	Gaussian distribution
A_n	Nominal area
h	Height of sinusoidal wave
L_2	Substrate length
S_Y	Yield strength
N	Number of meshing elements
P^*_{EP-H}	Elastic-plastic average contact pressure including hardening
S_E	Effective yield strength
$\overline{g_o}$	Normalized surface separation
f	Frequency

R	Asperity radius of curvature
z	Surface height
z_{ave}	Average surface height
a	contact radius
A_r	real area of contact
A_{JGH}	area of contact from model by Johnson et al. [20]
ω	interference between hemisphere and surface
$\bar{p}$	average pressure over entire surface

Chapter 1

INTRODUCTION

In most of every case of daily life we meet tribology phenomena. Any product where one material slides or rubs over another is affected by complex tribological interactions. Tribology is the science and engineering of interacting surfaces in relative motion and of related subjects and practices. It describes the phenomena of friction, wear, and lubrication. In the past, numerous authors studied rough surface. The classical analysis makes simplifying assumptions about the surface topography and deformation behavior. Traditionally, the surfaces were modelled analytically using assumptions and simplifications. The behavior of a single pair of interacting asperities was often extrapolated to describe the behavior of a pair of interacting rough surfaces covered in asperities.

Until nowadays, surface roughness effects were ignored in the analysis, due to the difficulty to generate a rough surface model and also to simplify the model in order to reduce computational time. However, many engineering fields seek to improve the behavior of the system at the surface level or interference between surfaces. Thus, with the advancement of numerical capabilities, the topography of the surface can be included in finite element simulations.

The study of contact mechanics has been realized as an important field for many years. All engineering surfaces are rough on the nano or micro-scale, therefore it is important to develop

model for the contact between rough surfaces. The problem of rough surface contact has existed for a long time. In order to understand the real mechanisms behind the interaction between the asperities or rough surfaces, different types of methods have been developed for modelling rough surface contact. The main objective to model the contact between rough surfaces is to find a simple closed form solution for the real contact area because most tribological parameters such as wear, adhesion, friction, contact resistance etc. are dependent on the real area of contact between the two surfaces in contact. The real contact area is a critical variable not only in this case but also in every dynamic system where two surfaces are brought together.

The main goal of this thesis is to study an elastic-plastic axisymmetric sinusoidal surface asperity in contact against a rigid flat with strain hardening. The non-linear isotropic hardening with two different laws is considered for the analysis by varying the hardening exponent ranging from $n = 0.1$-0.5. A Finite Element simulation was used to calculate the values of real contact area and contact pressure when two surfaces are in complete contact. The proposed model of the axisymmetric sinusoidal asperity in this thesis was generated using the Finite Element commercial software ANSYS^{TM} 17.1. Owing to the axisymmetric nature of the model makes it more computationally efficient as compared to other rough surface contact models. The results are curve fitted to provide an expression for the contact area over a wide range of cases. The results obtained from power law hardening are also compared with results obtained from Bilinear Hardening for $E_T = 1\%E, 2\%E, 5\%E, 10\%E$ in order to see the possible change in trend for two different types of hardening. For modelling real rough surface involves lots of computational time and complexity. However, modelling the single axisymmetric sinusoidal asperity can be a solution for both these problems.

2

1.1   Organization of thesis

- Chapter 2 of this thesis presents a thorough background on different types of contact models ranging from spherical shaped contact to sinusoidal shaped contact models.

- Chapter 3 of this thesis presents the modelling methodology employed in the formulation of the Finite element Model (FEM). This section is divided into three sections. The first section of this chapter describes how the solid model is built for the finite element analysis. The second section deals with the approach used for mesh convergence test. The third section deals with the methodology involved in performing the length convergence test.

- In Chapter 4 the results obtained for both the types of hardening are discussed.

- Chapter 5 concludes with the summary of this thesis.

Chapter 2

LITERATURE REVIEW

2.1   Introduction

The first objective of this chapter is to give an overview of a few of the many various contact mechanics techniques available. Each of these models is unique in its assumptions and mathematical techniques despite considerable qualitative agreement in their results. This chapter also elucidates various rough surface contact models such as statistical contact models, fractal contact models and multiscale contact models which will be discussed later in this chapter.

Most recent contact models consider a sinusoidal shape for the asperities because it seems to model the geometry of real surfaces better, especially for heavily loaded contacts [1-5]. It is shown for two-dimensional sinusoidal surfaces [6] and three-dimensional sinusoidal surfaces [7] that the average contact pressure increases past the conventional hardness, H, limit of $3 * S_y$ obtained by assuming spherical geometries [8]. Additionally, the current model is designed in such a way that it's axisymmetric and the interactions with the adjacent asperities are considered by the effect of periodicity at the base of asperity. Hence, it is logical to use a sinusoidal shape asperity instead of a spherical shape in modelling the asperities.

2.2   Spherical contact models

Most of the previous models on the contact between rough surfaces assume a spherical shape [9-16] or ellipsoidal shape [17-19] for the geometry of the asperities on the surfaces. The following

discussion may at first seem off topic, but in reality spherical contact is very significant for modelling sinusoidal asperities. Archard [10] used a stacked model of spherical asperities and showed that although the relation between the contact area and load for a single asperity is nonlinear, by using a multi-scale model this relation becomes linear.

Johnson et al. [20] provided two limiting solutions to three dimensional sinusoidal contacts. The first solution was based upon the Hertz elastic spherical contact solution. The Hertz solution provides closed-form expressions to the deformations and stresses of two spheres in purely elastic contact. The two spheres may different radii and elastic properties. However, the closed-form solutions render an equivalent case where a single elastic sphere, having an equivalent elastic modulus, denoted by E', and an equivalent radius, R, is in contact with the rigid flat. Fig. 2.1 is representing the cross section of a sinusoidal type of contact.
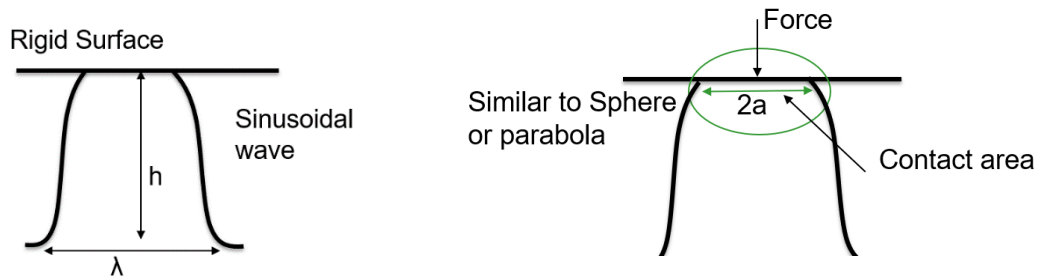
Fig. 2.1: Cross section of sinusoidal type contact

The Hertz solution assumes that the interference, ω, is small enough such that the geometry does not change significantly. The interference can be defined as the distance the sphere is displaced normally into the rigid flat. The resulting equation for contact radius and load from the Hertz solution are:

$$A_E = \pi R \omega \tag{2.1}$$

$$F_E = \frac{4}{3} E' \sqrt{R} (\omega)^{\frac{3}{2}} \tag{2.2}$$

where

$$\frac{1}{E'} = \left(\frac{1-v_1^2}{E_1}\right) + \left(\frac{1-v_2^2}{E_2}\right) \tag{2.3}$$

$$\frac{1}{R'} = \frac{1}{R_1} + \frac{1}{R_2} \tag{2.4}$$

Where E_i and v_i are the Young's modulus and Poisson's ratio respectively for the two bodies in contact and $i = 1, 2$. R_1 and R_2 are the radii of sphere 1 and 2 respectively.

2.3   Elastic sinusoidal contact

Some recent models consider a sinusoidal shape for the asperities because it seems to model the geometry of real surfaces better, especially for heavily loaded contacts [21-25]. The first models on the contact between rough surfaces using sinusoidal shaped asperities were mostly on the purely elastic contact. The elastic contact of two-dimensional sinusoidal surfaces was first solved by Westergaard [21]. Johnson et al. (JGH) [26] presented two asymptotic solutions for the elastic contact of three-dimensional sinusoidal surfaces, but no analytical solution is available for the entire load range. Jackson and Streator [27] developed an empirical equation based on the   JGH data [26] for the whole range of loading from early contact to

6

complete contact.

The analysis for the case of 3-D waviness in contact with a frictionless flat developed by Johnson, Greenwood and Higginson [20] (JGH model) provides a relation between pressure and contact area. In their work, $\bar{p}$ is defined as the average pressure on the surface (considering both contacting and non – contacting regions), and p^* is defined as the average pressure that when applied to the surface causes complete contact. One of the important stages in contact between the surfaces is when "complete contact" happens. The definition of complete contact between rough surfaces depends on the specific cases and geometry of the surfaces in contact. For sinusoidal surfaces, it is defined as the state in which sinusoidal surfaces have completely flattened out and there is no gap in between the surfaces. The expression for p^* is given by Eq. (2.5).

$$p^* = \sqrt{2}\,\pi E'\Delta f \tag{2.5}$$

where E' is the equivalent elastic modulus, Δ is the amplitude of the sinusoidal surface, and f is the frequency or reciprocal of wavelength, λ. Thus when $\bar{p} \geq p^*$, the pressure loads the surfaces so that there is no gap between them. Alternatively, when $\bar{p} < p^*$ the contact is not complete, and a closed form solution for the three-dimensional waviness contact problem is not available. However, Johnson et al. [20] provides two asymptotic solutions to the problem. For $\bar{p} \ll p^*$ the following equation derived from Hertz contact theory applies:

$$(\bar{A}_{JGH})_1 = \frac{\pi}{f^2}\left[\frac{3}{8\pi}\frac{\bar{p}}{p^*}\right]^{\frac{2}{3}} \tag{2.6}$$

And when $\bar{p}$ approaches p^* i.e. contact is nearly complete the following equation applies:

$$(\bar{A}_{JGH})_2 = \frac{1}{f^2}\left(1 - \frac{3}{2\pi}\left[1 - \frac{\bar{p}}{p^*}\right]\right) \tag{2.7}$$

Since the general analytical solution is not available, Jackson and Streator gave an equation, which was based on the experimental and numerical data offered by Johnson, to connect the two cases above and are given by.

For $\frac{\bar{p}}{p^*} < 0.8$:

$$\bar{A} = \left(\bar{A}_{JGH}\right)_1\left(1 - \left[\frac{\bar{p}}{p^*}\right]^{1.51}\right) + (\bar{A}_{JGH})_2\left(\frac{\bar{p}}{p^*}\right)^{1.04} \tag{2.8}$$

For $\frac{\bar{p}}{p^*} \geq 0.8$:

$$\bar{A} = (\bar{A}_{JGH})_2 \tag{2.9}$$

2.4   Elasto-plastic sinusoidal contact

Three-dimensional elasto-plastic sinusoidal contact has been investigated by Krithivasan and Jackson [24] and Jackson et al. [25]. They proved that for the elasto-plastic sinusoidal contact, They also found that complete contact occurs much earlier at lower pressures than elastic contact. Jackson et al. [25] presented an empirical equation for calculating the average pressure, p^*_{ep}, that causes complete contact to occur for elasto-plastic case. The equation is given below:

$$\frac{p_{ep}^*}{p^*} = \left(\frac{11}{4\left(\Delta/\Delta_c\right)+7}\right)^{3/5} \tag{2.10}$$

Where Δ_c is the analytically derived critical interference, and is given by:

$$\Delta_c = \frac{\sqrt{2}s_y e^{2/3v}}{3\pi E' f} \tag{2.11}$$

Jackson and Krithivasan's [24] empirical equation for contact area vs contact pressure for elasto-plastic case is given by:

$$A = \left(A_p\right)\left(1 - \left[\frac{\bar{p}}{p_p^*}\right]^{1.51}\right) + \left(\bar{A}_{JGH}\right)_2 \left(\frac{\bar{p}}{p_p^*}\right)^{1.04} \tag{2.12}$$

Where A_p is given by

$$A_p = 2(A_c)^{\frac{1}{1+d}}\left(\frac{3\bar{p}}{4Cs_y f^2}\right)^{\frac{d}{1+d}} \tag{2.13}$$

In Equation 2.13, A_c is the critical contact area for the sinusoidal contact based on spherical contact [28], and is given by:

$$A_c = \frac{2}{\pi}\left(\frac{Cs_y}{8\Delta f^2 E'}\right)^2 \tag{2.14}$$

Where the constant C is related to the Poisson's ratio by:

$$C = 1.295 \exp(0.736v) \tag{2.15}$$

The value of the constant d in Eq. 2.13 is given by:

$$d = 3.8\left(\frac{E'}{s_y}\Delta f\right)^{0.11} \tag{2.16}$$

2.5   Statistical rough surface contact model

One of the earliest works in the field of contact mechanics has been credited to Heinrich Hertz back in 1882. Based upon the findings of interference fringes between the glass lenses, his

work displayed elastic displacement in surfaces that were compatible with his proposed elliptical pressure distribution. Since these findings, many contact models have been developed to expand the Hertzian contact solution from a single asperity or raised portion on a surface into a distribution of network of related asperities that can more accurately describe the topography of rough surfaces.

The statistical model is an important type of model in analyzing rough surface contact problems. In 1966, Greenwood and Williamson [29] devised a rough surface contact model here referred to as the GW model. The primary assumptions of this model are that all the asperities must have same radius of curvature, each asperity must behaves independently of its neighbors, and the substrate material is not allowed to deform. Greenwood and Williamson first introduced the statistical approaches to characterize the surface topography in contact mechanics. The Statistical method has long been considered as an easy and simple approach to model rough surface contact. However this model has a few shortcomings such as the dependence of spectral moments on the resolution of the surface measuring apparatus and the sample length [30 -31].

Greenwood and Williamson [29] showed that rough surfaces can be modelled as a set of mutually exclusive asperities with contant radii and a variable height based on a particular height distribution function. A Gaussian distribution, $\Phi(z)$, is usually assumed for the height distribution. The contact parameters of rough surfaces are obtained from the equations below:

$$A(d) = \eta A_n \int_d^\infty \bar{A}\,(z - d)\Phi(z)dz \qquad\qquad (2.17)$$

$$P(d) = \eta A_n \int_d^\infty \bar{P}\,(z - d)\Phi(z)dz \qquad\qquad (2.18)$$

where A_n is the nominal or apparent area of contact, which is defined by the overlap of surfaces in contact, $\bar{A}$ is the individual asperity contact area, $\bar{P}$ is the corresponding contact load. d is defined as the value above which the asperities will be in contact with the rigid flat (i.e. the mean surface separation). The compression distance, $z - d$, is the interference of the rigid flat with the asperity peaks. For the perfectly elastic case, $\bar{A}$ and $\bar{P}$ are acquired from the Hertz solutions given by Eq. 2.1 and Eq. 2.2.

2.6   Fractal Rough Surface Contact Model

Although the fractal contact model captures the surface topography in a multi-scale nature, it is important to note that not all engineering surfaces have profiles which exhibit exact fractal behavior. In order to overcome the drawback of spectral moment dependence on surface parameters in the statistical models, the fractal model proves beneficial to characterize the surface topography.

In 1991, Majumdar and Bhushan [32] developed a well-known contact model that is based on fractal roughness parameters. Through course of their work, they found that a surface is multiscale in nature in that as a surface is viewed with higher magnification, each new "scale" will show a topographical roughness. Their work suggested that surfaces are structurally fractal, thus, the statistical parameters are scale-dependent. They used a geometric truncation between a fractal surface and a flat to calculate contact area and spot size. They also presented that the fractal roughness parameters significantly influenced the relation between the contact load and the real contact area. The dimensionless total contact load is given by:

$$F^* = \frac{4\sqrt{\pi}}{3} G^{*(D-1)} g_1(D) A_r^{*\frac{D}{2}} \left[\left(\frac{(2-D)A_r^*}{D} \right)^{(3-2D)/2} - a_c^{*\frac{(3-2D)}{2}} \right]$$

$$+ K\phi g_2(D) A_r^{*\frac{D}{2}} a_c^{*\frac{(2-D)}{2}}$$

(2.19)

where

$$g_1(D) = \frac{D}{3-2D} \left(\frac{2-D}{D} \right)^{D/2} \ ; \ g_2(D) = \left(\frac{D}{2-D} \right)^{(2-D)/2}$$

(2.20)

$$A_r^* = \frac{A_r}{A_a}; \ a_c^* = \frac{a_c}{A_a}$$

(2.21)

G and D in the Eq. 2.21 are fractal roughness parameter and fractal dimension of a surface profile, respectively. They can be obtained from the W-M function's power spectrum

$$S(w) = \frac{G^{2(D-1)}}{2ln\gamma} \frac{1}{\omega^{(5-2D)}}$$

(2.22)

where $S(w)$ is the power spectrum and ω represents the frequency. Manjumdar and Bhusan [36] have extensively used fractal methods to characterize surface topography and also in scale dependent rough surface contact models. Chapter 3 discusses about the steps followed for building the solid finite element model.

Chapter 3

FINITE ELEMENT MODEL

3.1   Introduction

This chapter describes in detail the methodology employed in building the solid finite element model. The model is divided into two parts. The first part is the rigid flat surface that acts as the contact surface and the second being the sinusoidal surface on which the target elements are created. This section also discusses the methodology used for mesh convergence test and length convergence test.

3.2   Building the solid model

The current analysis will examine the case of axisymmetric elastic-plastic sinusoidal surface asperity contact against a rigid flat with strain hardening by conducting the parametric study using the finite element method. The present model uses an axisymmetric sinusoidal surface and the profile of this surface is described by

$$h = \Delta\left(1 + \cos\left(\frac{2\pi r}{\lambda}\right)\right), 0 \leq r \leq \frac{\lambda}{2} \tag{3.1}$$

Where h is the height of the sinusoidal surface and r is the radius of the sinusoidal surface, and λ is the wavelength of the sinusoidal wave. This work uses the same approach used by Saha and Jackson [33] for modelling the elastic-plastic case for axisymmetric sinusoidal contact without considering the strain hardening. A 3- dimensional rendering of geometry used in this thesis and is described by Fig. 3.1.
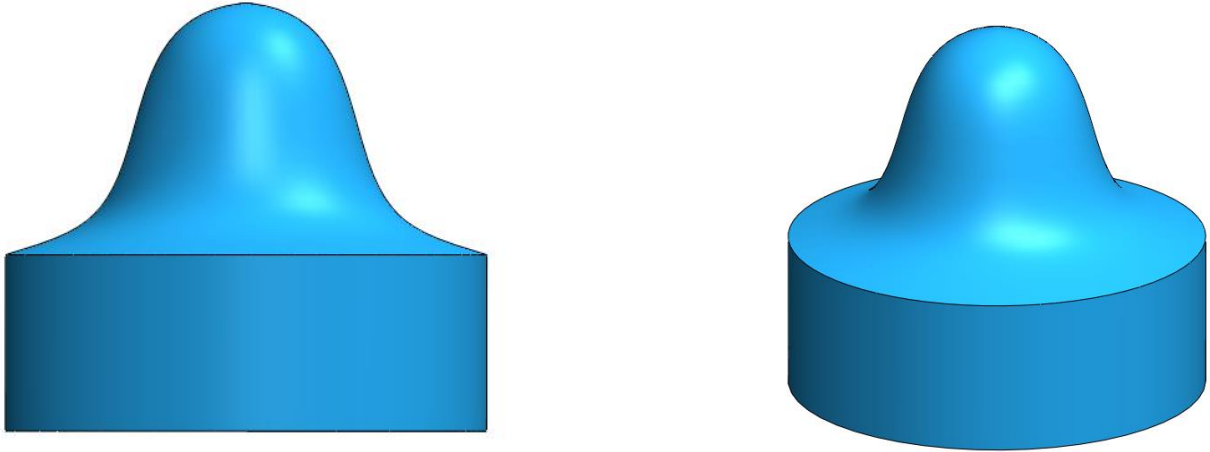
Fig. 3.1: Three-dimensional view of the surface of an axisymmetric sinusoidal asperity

The commercial ANSYS™ 17.1 package with APDL coding was used to model the elastic-plastic contact of a sinusoidal surface loaded against a rigid flat with strain hardening. APDL stands for "ANSYS Parametric Design Language" is an alternative to the GUI (Graphical User Interface) to perform modelling in ANSYS. Since generating a sinusoidal asperity via GUI in ANSYS is very tedious, we used APDL instead. Owing to the axisymmetric nature of the sinusoidal surface (shown in Fig. 3.1), only the right half section (a 2-D axisymmetric section) of the model was rendered in the finite element analysis within the period of r = [0,R]. For meshing the entire sinusoidal surface and it's substrate, a PLANE 183 (8-node plane element with mid nodes) was employed. CONTA 172 (3-node contact element with a mid- node), was used on the rigid flat surface and TARGE 169 (2-node contact element) , was used over the sinusoidal surface.

The contact was also assumed to be frictionless and the contact elements used the Augmented Lagrange Method for enforcing contact and limiting penetration between the surfaces. The Augmented Lagrange Method is very similar to the pure penalty method, but it adjusts the contact force with a constant that is independent of the penetration stiffness.

3.3 Boundary Conditions

The boundary conditions (BC's) that are considered in the present study are:

- The rigid flat only translates in the y direction.

- Displacements U_x and U_y in both the x and y directions are fixed on the bottom of the substrate.

- $U_x(0, y) = 0$ $i.e.$ the axisymmetric boundary condition is applied at the axis of symmetry.

- Boundary conditions that consider interaction with adjacent asperities are applied to the displacements in the radial direction along the substrate length, L_2, such that $U_x\left(\frac{-\lambda}{2}, y\right) = U_x\left(\frac{\lambda}{2}, y\right) = 0$.

The displacement method was employed to simulate the contact problem. This method applies a finite displacement to the rigid flat surface in the y- direction toward the sinusoidal surface, and then solves the contact problem. The flat rigid surface was constrained to move only along the y axis. Additionally, displacements at the bottom of the substrate in both the x and y directions were set to zero (i.e. $U_x = 0$ and $U_y = 0$). The simulation methodology can be understood better from Fig. 3.2.
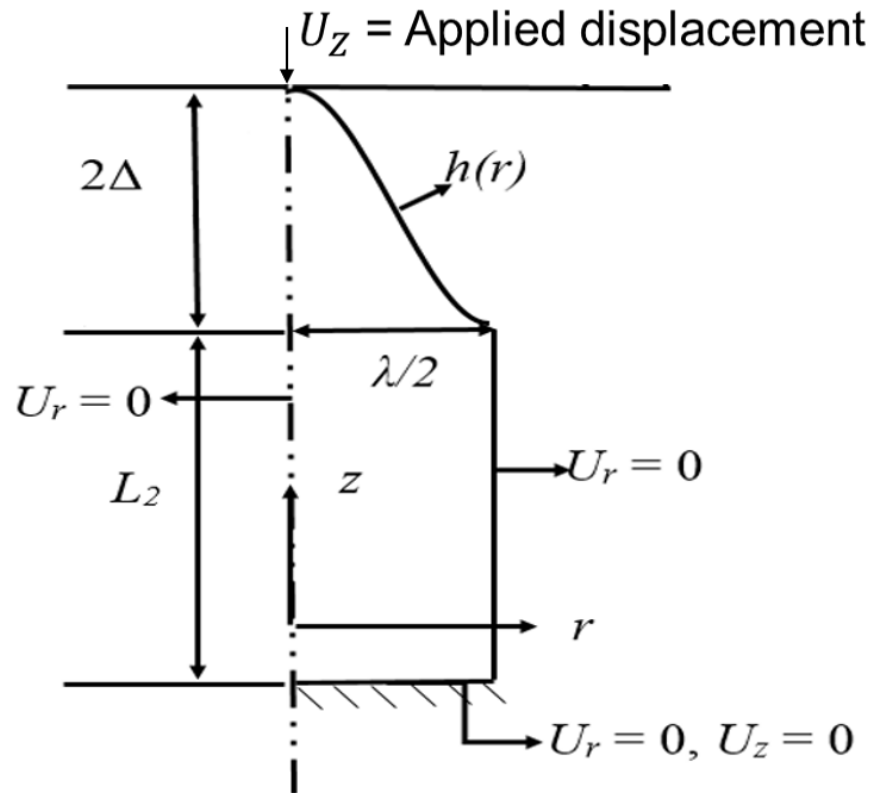
Fig. 3.2: Schematic of an axisymmetric sinusoidal asperity loaded against a rigid flat [33].

3.4   Normalization

Through the course of the work, it was found that one other normalization scheme actually appears better at collapsing the data onto a universal curve. As is done in previous works on elasto-plastic contact, the contact area and the pressure obtained from the finite element results can be normalized by the following expression:

$$A^* = \frac{A_{FEM}}{A_c} = \frac{A_{FEM}}{\pi R^2} \tag{3.2}$$

where A_{FEM} is the contact area obtained from the finite element model and R is the radius of the sinusoidal wave. Since, only the right half of the sinusoidal wave was used in the finite element model, so radius of the sinusoidal wave can be defined as $R = \frac{\lambda}{2}$.

The pressure required for complete contact was then normalized by the following expression:

$$P^* = \frac{F_{FEM}}{\pi R^2 E' \frac{\Delta}{\lambda}} \tag{3.3}$$

where F_{FEM} is the force obtained from the finite element model, E' is the equivalent elastic modulus, Δ is the amplitude of the sinusoidal wave, and λ is the wavelength of the sinusoidal wave.

3.5   Mesh Convergence Test

The number of elements was increased iteratively by a factor of 1.8-2, by gradually increasing the nodal density, especially ones that are close to the contact interface until mesh convergence was obtained. Separate mesh convergence test were performed for power law hardening and bi-linear hardening in order to see the possible change in results for two different types of hardening on a same model.

For power law hardening, it is observed that a total number of 74,200 elements produces results that satisfy mesh convergence. It is obvious that any further increase in the number of elements does not affect the results. The finite element model associated with this number of elements is used throughout the rest of the study while keeping the other parameters involved constant. The mesh convergence test was only performed for the minimum and maximum value of the power law hardening exponent (i.e. $n = 0.1$ and $n = 0.5$) by assuming that it will not change for the intermediate values of hardening exponent.

A Similar approach was used to perform the mesh convergence test for bilinear hardening. For bi-linear hardening 107,152 elements produces reasonable results. The mesh convergence test was only performed for $E_T = 1\%E$ and $E_T = 10\%E$ by assuming that it will not change for the other in between values of tangent modulus. A Similar approach was then used to perform the mesh convergence test whenever the Δ/λ ratio was changed. Results obtained for mesh convergence for different cases are discussed below. Fig. 3.3 shows the mesh for different number of elements for sinusoidal asperity in contact with rigid flat for $\lambda = 1\ mm$ and $\Delta = 0.005\ mm.$
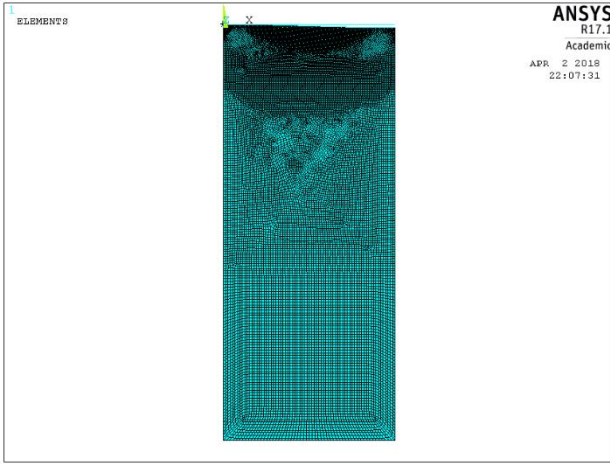
N = 21526 elements   N = 48052 elements
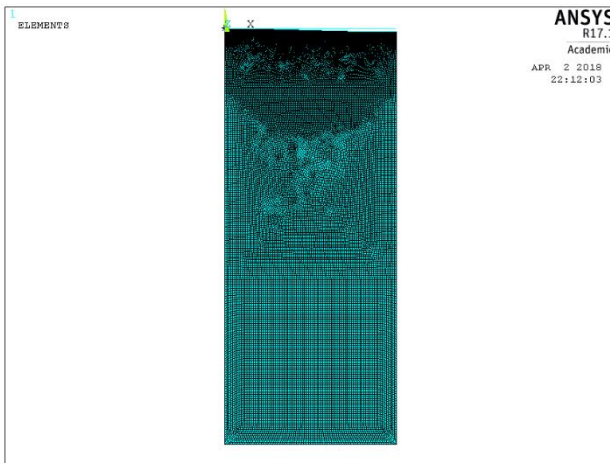
N = 74200 elements   N = 131276 elements

Fig. 3.3: Mesh of sinusoidal asperity in contact with rigid flat for $\lambda = 1\ mm$, $L_2 = 1.2\ mm$ and

$\Delta = 0.005\ mm$ for different number of elements.

N = 21526 elements
N = 48052 elements
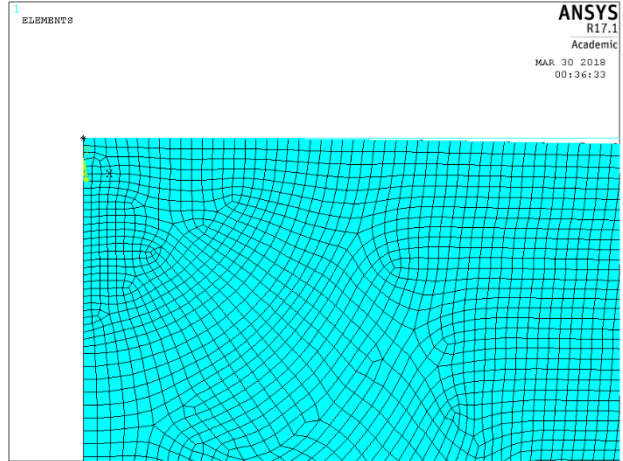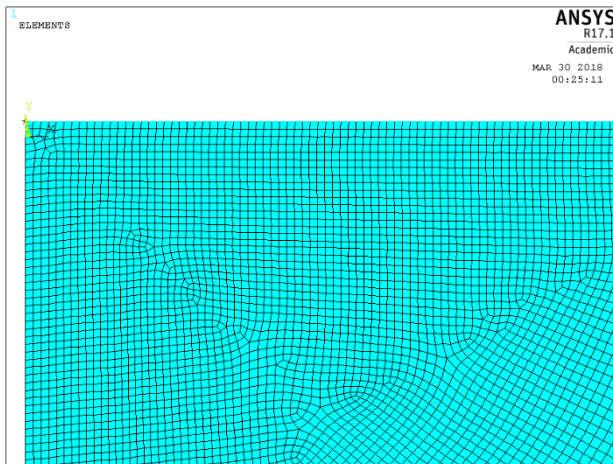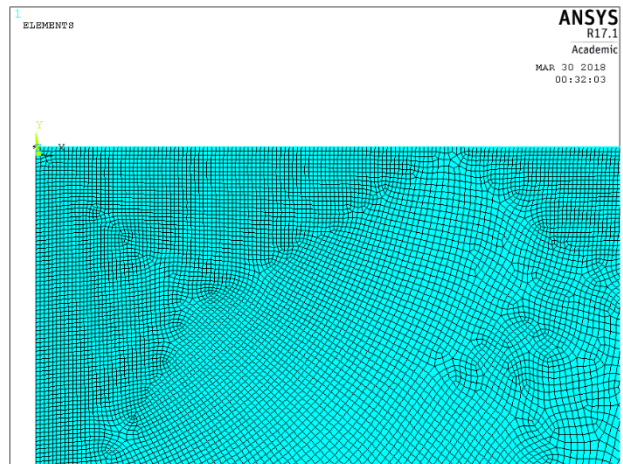
N = 74200 elements
N = 131276 elements

Fig. 3.4: Zoomed Mesh of sinusoidal asperity in contact with rigid flat for $\lambda = 1\ mm$, $L_2 = 1.2$ mm and $\Delta = 0.005\ mm$.

3.6 Mesh Test Plots for Power Law Hardening ($E/S_Y = 200, \Delta = 0.005\ mm$)

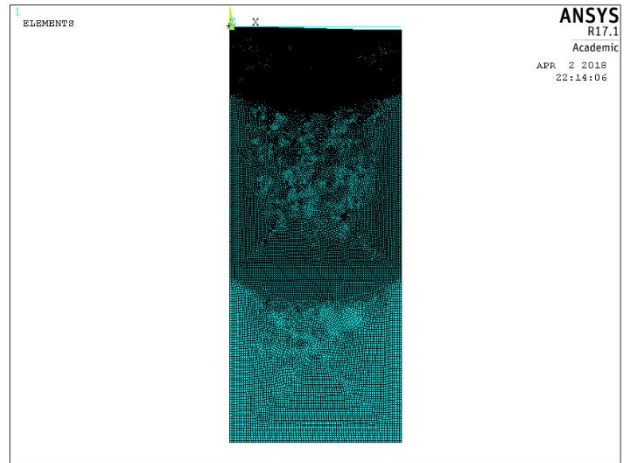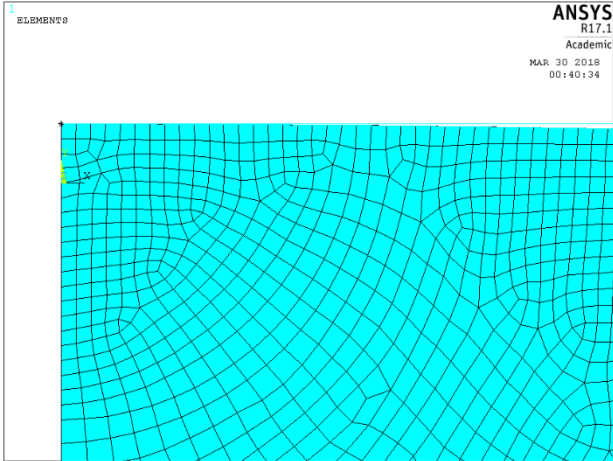At complete contact, an average error of 0.05% between the meshes of 74,200 and 131,276 elements was obtained from the mesh convergence plot for $n = 0.1$, and an average error of 0% between the meshes of 74,200 and 131,276 elements was obtained from the mesh convergence plot for $n = 0.5$. Fig. 3.5 and Fig. 3.6 shows the mesh convergence test for $n = 0.1$ and $n = 0.5$ respectively. The same number of elements was then used for obtaining the results for intermediate values of hardening exponent by assuming that the mesh convergence results will not change. A similar approach was then used for the mesh convergence test for $E/S_Y = 20$ and $E/S_Y = 2000$ by keeping the other parameters constant. Finally, 74,200 elements was used for meshing due to the low error value. The material properties used to perform the mesh convergence tests are given in Table 3.1.

Table 3.1: Material Properties for mesh convergence test (Power Law Hardening)

Elastic Modulus	S_Y	E/S_Y	Substrate Length (L_2)	Δ	λ
200E3 N/mm^2	1000 N/mm^2	200	1.2 mm	0.005 mm	1 mm
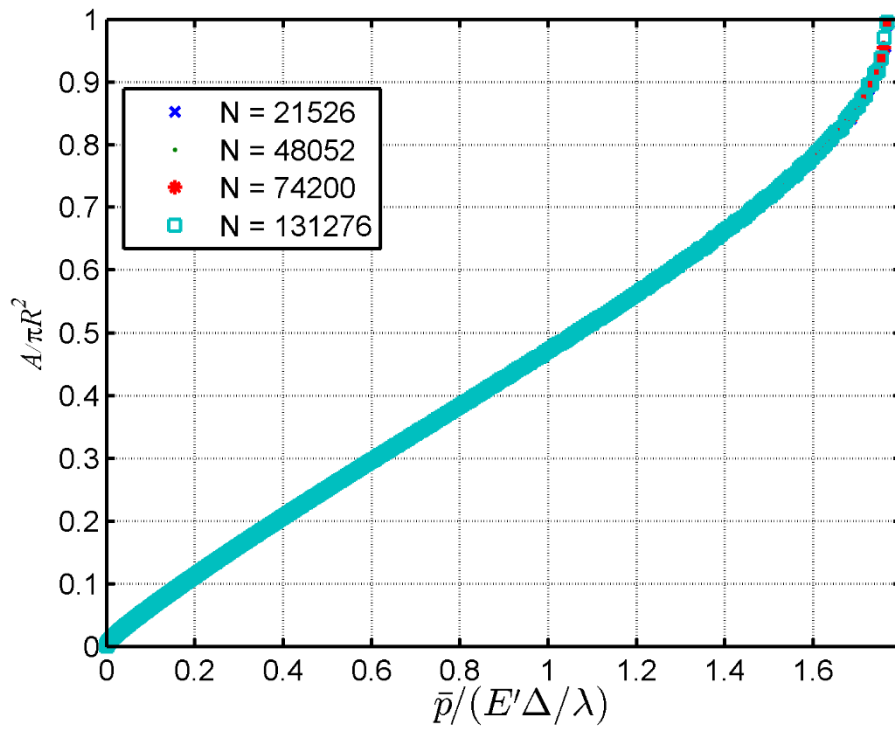
Fig. 3.5: Mesh convergence test for n = 0.1 and E/S_Y = 200
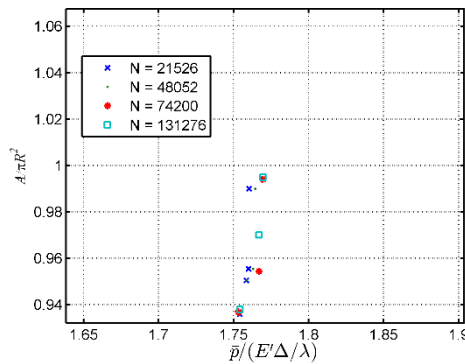
Zoomed view at complete contact

Fig. 3.6: Mesh convergence test for $n = 0.5$ and $E/S_Y = 200$

Zoomed view at complete contact

3.7 Mesh Test Plots for Bilinear Hardening $\left(E/S_Y = 2000, \Delta = 0.0005\ mm\right)$

At complete contact, an average error of 1.07% between the meshes of 41,209 and 151,980 elements was obtained from the mesh convergence plot for $E_T = 1\%E$, and an average error of 0.69% between the meshes of 107,152 and 151,980 elements was obtained from the mesh convergence plot for $E_T = 10\%E$. Fig. 3.7 and Fig. 3.8 shows the mesh convergence test for $E_T = 1\%E$ and $E_T = 10\%E$ respectively. Finally, 151,980 elements for $E_T = 1\%E$, and 107,152 elements for rest values of tangent modulus was then used for meshing due to low error value. A Similar approach was then used for the mesh convergence test for $E/S_Y = 200$ by keeping the other parameters constant. The material properties used to perform the mesh test are given in Table 3.2.

Table 3.2: Material Properties for mesh convergence test (Bilinear Hardening)

| Elastic Modulus	S_Y	E/S_Y	Substrate Length (L_2)	Δ	λ
200E3 N/mm^2	100 N/mm^2	2000	1.2 mm	0.0005 mm	1 mm
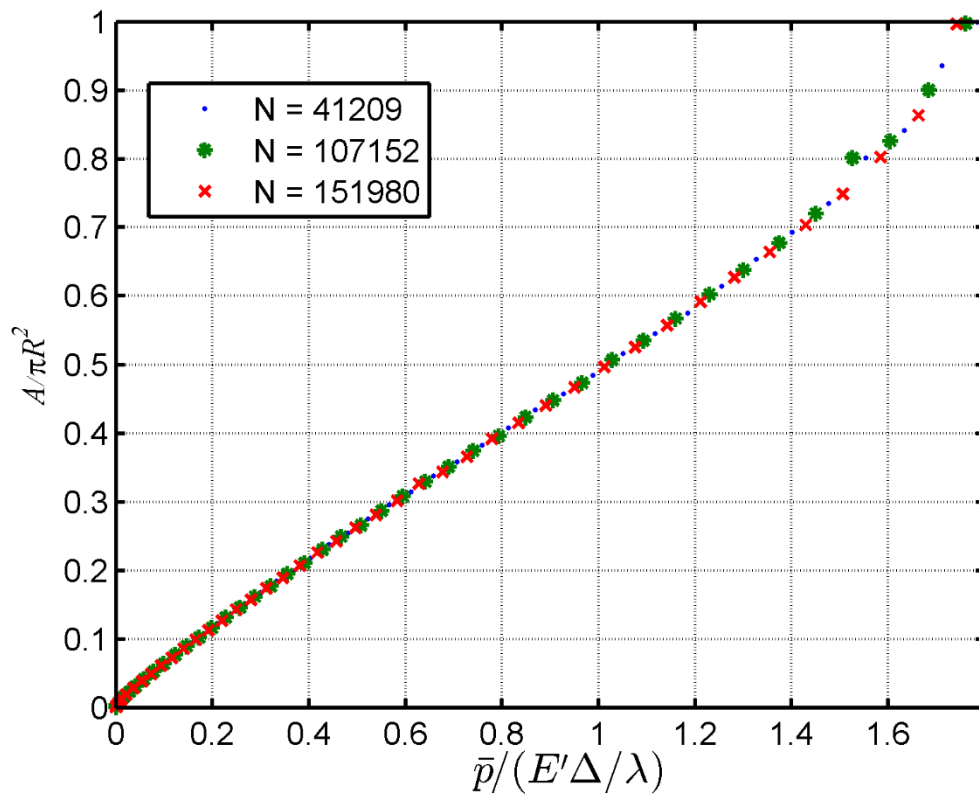
Fig. 3.7: Mesh convergence test for $E_T = 1\%E$ and $E/S_Y = 2000$
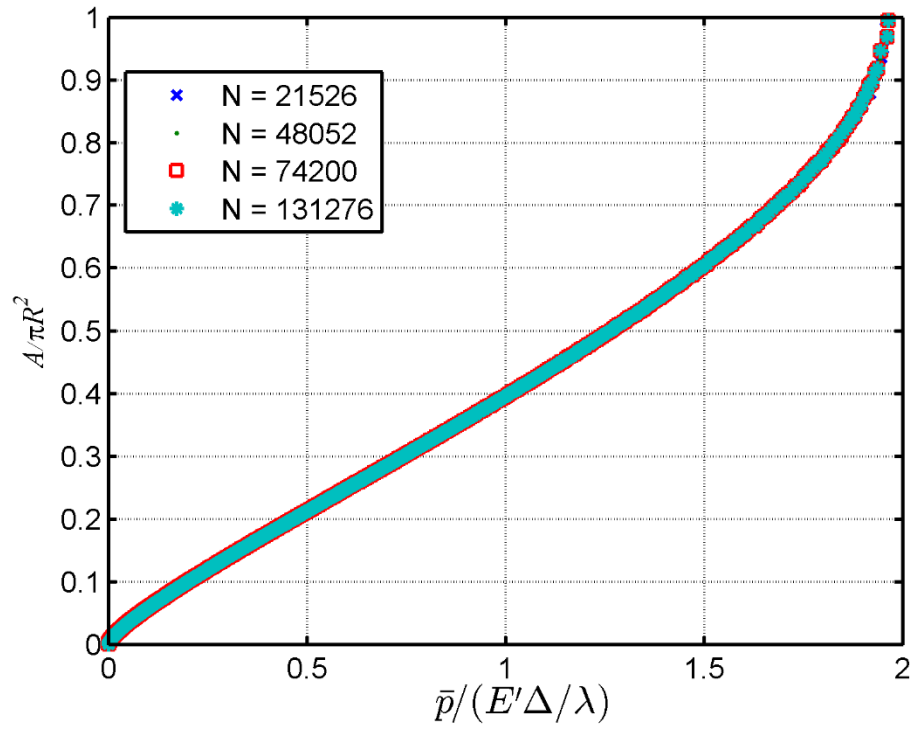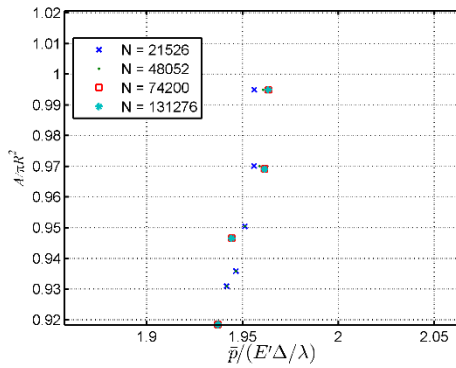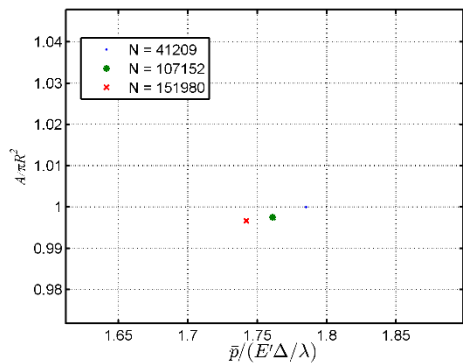

Zoomed view at complete contact
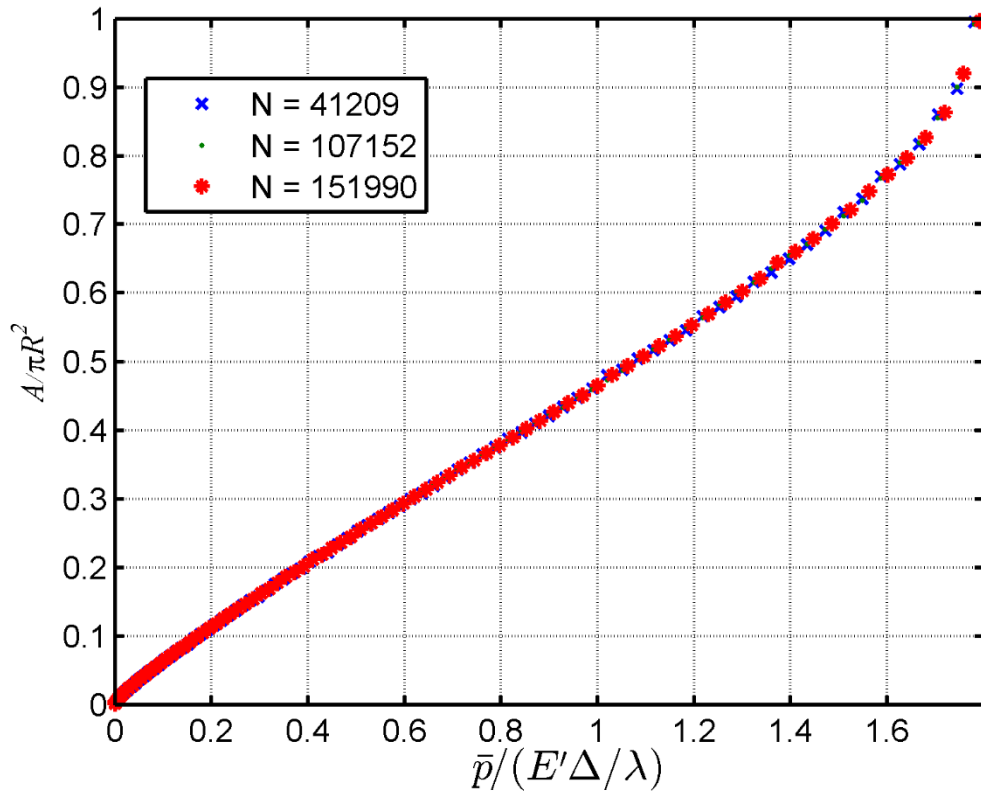
Fig. 3.8: Mesh convergence test for $E_T = 10\%E$ and $E/S_Y = 2000$
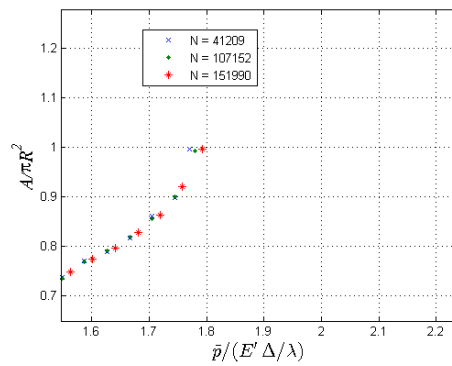
Zoomed view at complete contact

3.8   Length Convergence Test for Power law and Bilinear Hardening

In order to make the current model a semi infinite object length convergence test was performed so that half space equilibrium is reached and also to find out the length at which there will be no effect of load. For length (L_2) convergence test, three different values for the substrate length was varied (L_2 = 0.6 mm, L_2 = 1.2 mm, L_2 = 3 mm). The length convergence test was only performed for the minimum and maximum value of hardening exponent (i.e. n = 0.1 and n = 0.5) and (E_T = 1%E and E_T = 10%E) by assuming that it will not change for the intermediate values of hardening exponent and tangent modulus. Finally, L_2 = 1.2 mm was used as a substrate length. The material properties used to perform the length test for power law hardening are given in Table 3.3. Fig. 3.9 and Fig. 3.10 are representing the plots for length test for power law hardening.

Table 3.3: Material Properties for Length convergence test (Power law Hardening)

Elastic Modulus	S_Y	E/S_Y	Number of Elements	Δ	λ
200E3 N/mm^2	1000 N/mm^2	200	74200	0.005 mm	1 mm
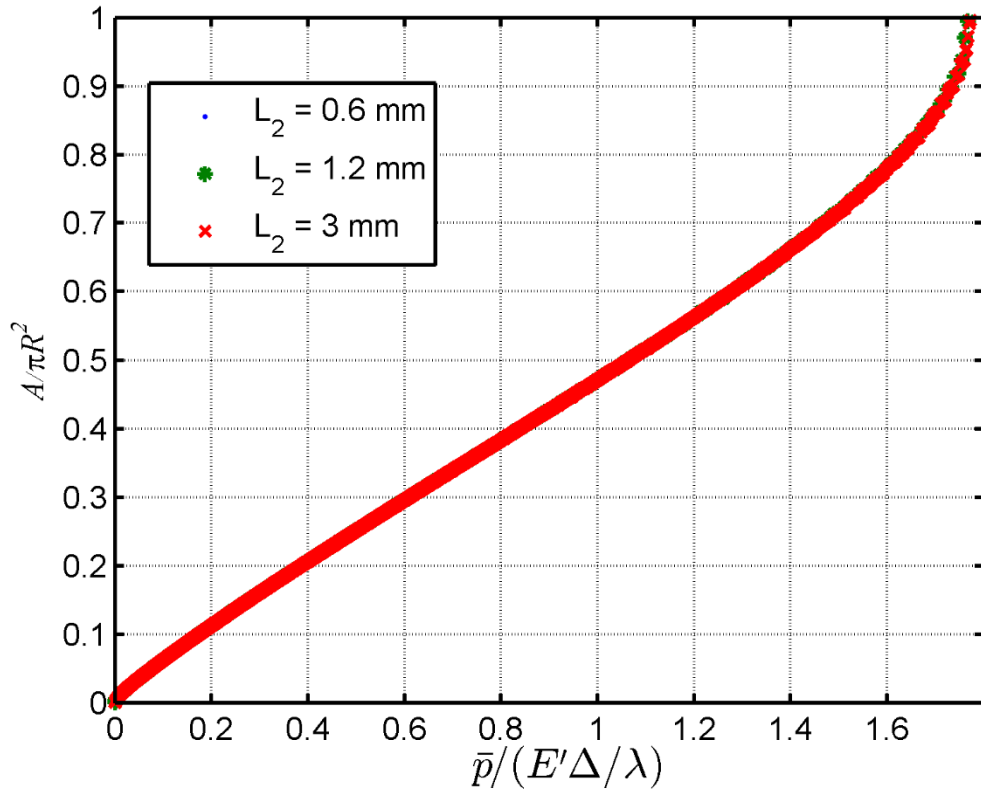
Fig. 3.9: Length convergence test for $n = 0.1$ and $E/S_Y = 200$
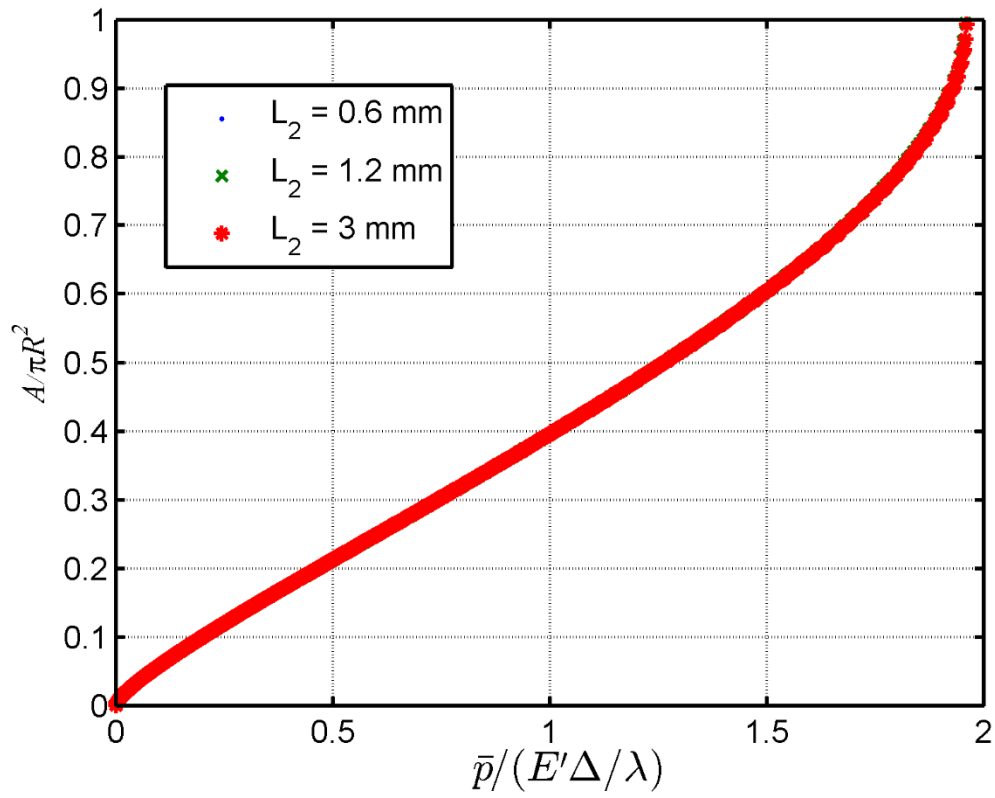
Fig. 3.10: Length convergence test for $n = 0.5$ and $E/S_Y = 200$

After analyzing the plot for $n = 0.1$ (Fig.3.9) at complete contact, an error of 0.19% was calculated between the results for $L_2 = 0.6$ mm and $L_2 = 3$ mm and an error of 0.32% was calculated between the results for $L_2 = 1.2$ mm and $L_2 = 3$ mm. Similarly, after analyzing the plot for $n = 0.5$ (Fig. 3.10), at complete contact an error of 0.13% was calculated between the results for $L_2 = 0.6$ mm and $L_2 = 3$ mm and an error of 0.1% was calculated between the results for $L_2 = 1.2$ mm and $L_2 = 3$ mm. Hence, $L_2 = 1.2$ mm was then considered as final substrate length due to low error value. Finally, for N = 74200 and $L_2 = 1.2$ mm a number of different cases by varying the hardening exponent (n) were then analyzed for $E/S_Y = 20$, $E/S_Y = 200$ and $E/S_Y = 2000$. A Similar approach was then used for a length convergence test for $E/S_Y = 20$ and $E/S_Y = 2000$. The material properties used to perform the Length test for bilinear hardening are given in Table 3.4. Fig. 3.11 and Fig. 3.12 are representing the plots of length test for bilinear hardening.

Table 3.4: Material Properties for Length convergence test (Bilinear Hardening)

Elastic Modulus	S_Y	E/S_Y	Number of Elements	Δ	λ
200E3 N/mm^2	100 N/mm^2	2000	107152	0.0005 mm	1 mm
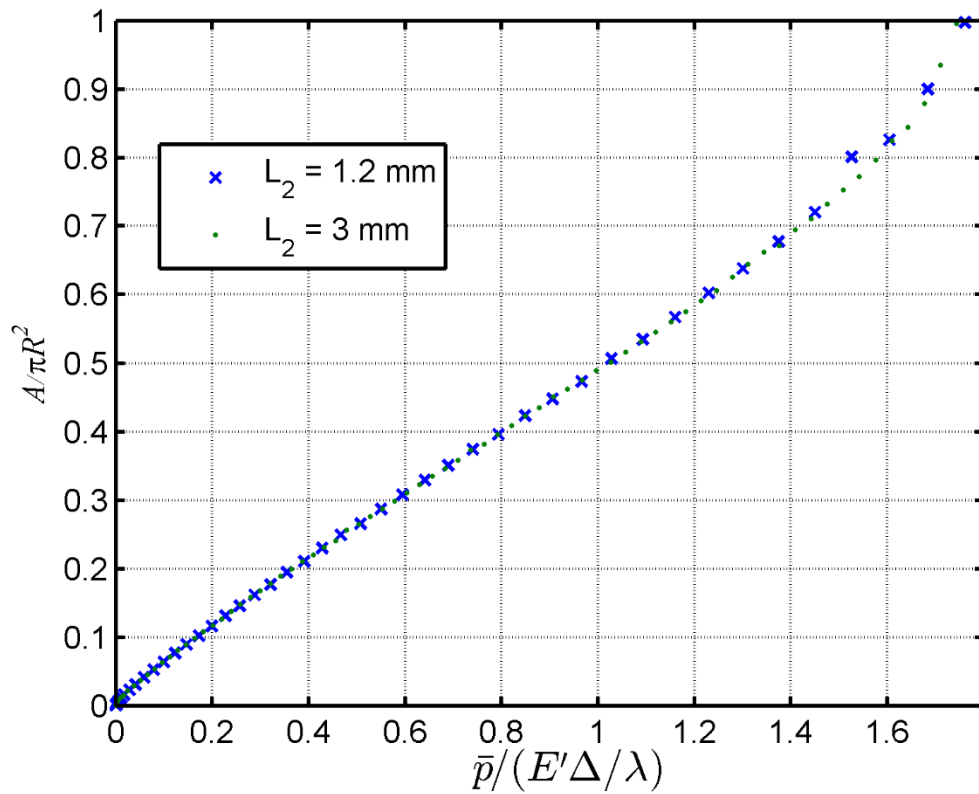
Fig. 3.11: Length convergence test for $E_T = 1\%E$ and $E/S_Y = 2000$
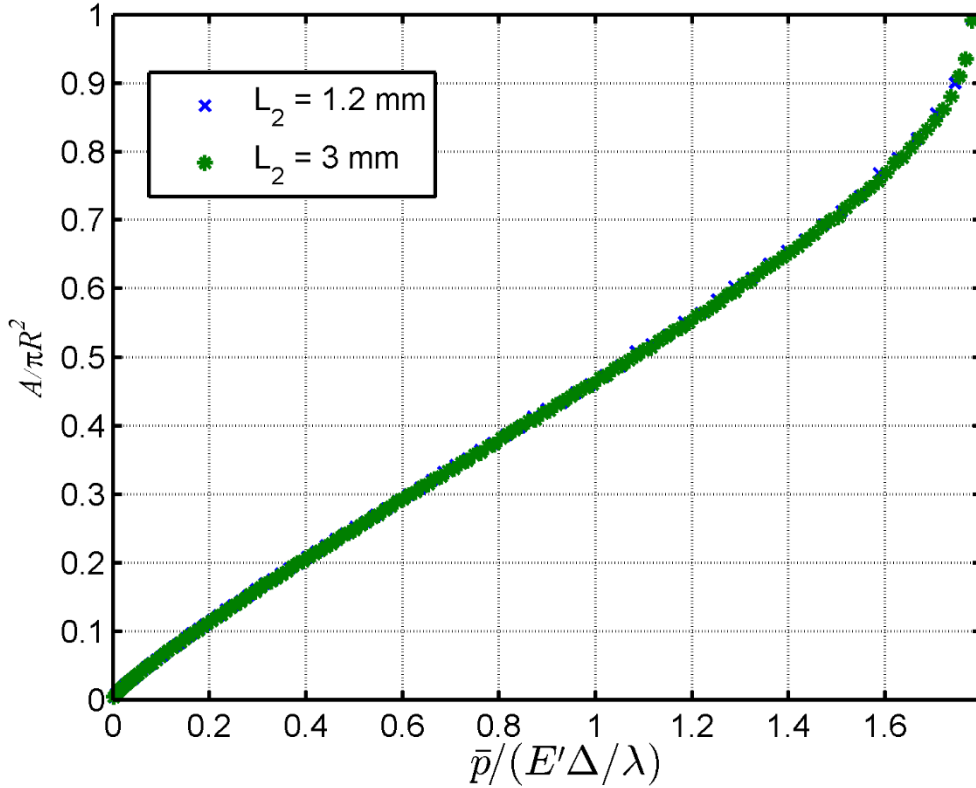
Fig. 3.12: Length convergence test for $E_T = 10\%E$ and $E/S_Y = 2000$

After analyzing the plot for $E_T = 1\%E$ (Fig. 3.11), at complete contact an error of 0.97% was calculated between the results for $L_2 = 1.2$ mm and $L_2 = 3$ mm. Similarly, after analyzing the plot for $E_T = 10\%E$ (Fig. 3.12), at complete contact an error of 0.02% was calculated between the results for $L_2 = 1.2$ mm and $L_2 = 3$ mm. Hence, $L_2 = 1.2$ mm was then considered as the final substrate length due to low error value. Finally, for N = 107,152 and $L_2 = 1.2$ mm a number of different cases by varying tangent modulus was then analyzed for $E/S_Y = 2000$. A Similar methodology was then used to perform the length convergence test for power law hardening using the same parameters discussed in Table 3.3. Table 3.5 and Table 3.6 shows the summary of the

final parameters used for mesh and length convergence tests for power law and bilinear hardening respectively.

Table 3.5: Summary of number of elements for power law hardening

E/S_Y	n	$\dfrac{\Delta}{\lambda}$	N	L
20	0.1-0.5	0.005	74,200	1.2 mm
200	0.1-0.5	0.005	74,200	1.2 mm
2000	0.1-0.5	0.005	74,200	1.2 mm
2000	0.1-0.5	0.0005	74,200	1.2 mm

Table 3.6: Summary of number of elements for bilinear hardening

E/S_Y	$\dfrac{\Delta}{\lambda}$	E_T/E			
		1%	2%	5%	10%
200	0.005	107,152	107,152	107,152	107,152
2000	0.005	107,152	107,152	107,152	107,152
2000	0.0005	151,980	107,152	107,152	107,152

In this chapter, details of numerical simulations are discussed. First, the methodology of building the solid model in commercial software $ANSYS^{TM}$ by using the finite element method is discussed. The second part of the chapter was focused on the approach followed for performing the mesh and length convergence test for both the power law and Bi-Linear hardening. Results Obtained from these simulation is discussed in Chapter 4.

Chapter 4

Finite Element Results and Comparison

4.1   Introduction

The material of the sinusoidal surface was assumed to be elastic-plastic isotropic power law hardening with a hardening exponent ranging from $n = 0.1 \leq n \leq 0.5$. The results obtained from power law hardening are also compared with the results obtained from bi-linear isotropic hardening for $E_T = 1\%E, 2\%E, 5\%E, 10\%E$. This chapter also discusses the hardening effect from the plots obtained from FEM results for both of the types of hardening.

Results and Discussions

4.2   Power Law Hardening

For the modelling of an elastic-plastic axisymmetric sinusoidal surface, different values of material properties were considered. In the current model, two different values of amplitude ($\Delta = 0.005$ mm and $\Delta = 0.0005$ mm) was assumed and the wavelength ($\lambda = 1$ mm) was used throughout the calculation. Then, the analysis was done for a fixed value of Young's modulus ($E = 200$ GPa) and for three different values of $E/S_Y = 20$, 200, 2000. Different values of the hardening exponent ranging from $n = 0.1 - 0.5$ were considered. Finally, for each E/S_Y ratio, all the results were plotted on a single plot for different values of the hardening exponent ranging, from $n = 0.1$, 0.15, 0.2, 0.25, 0.3, 0.35, 0.4, 0.45, 0.5. In order to check the hardening effect below the typical range of the hardening exponent (n), few more cases for each E/S_Y ratio and for two different

values of the hardening exponent $n = 0.01$ and 0.001 was then analyzed. The results obtained from each case are discussed below in detail. The equation for power law hardening is given by:

$$\sigma_Y / \sigma_O = \left(\sigma_Y / \sigma_O + 3G\widehat{\varepsilon^{pl}} / \sigma_o \right)^N \tag{4.1}$$

Where ε^{pl} is plastic strain, N is strain hardening exponent and G is shear modulus. The plots below are showing the stress vs strain relationship for the material properties used in the analysis.
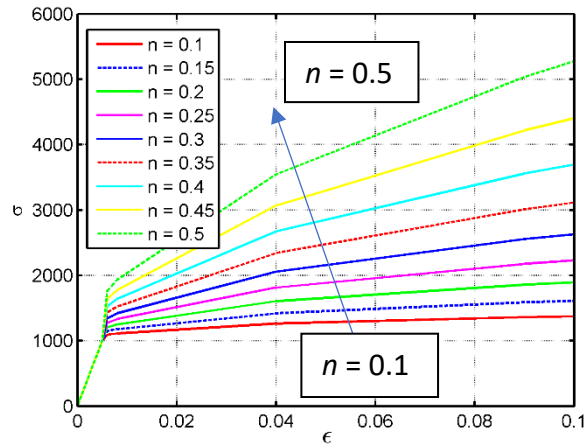
Fig 4.1: Stress vs strain for $E / S_Y = 200$
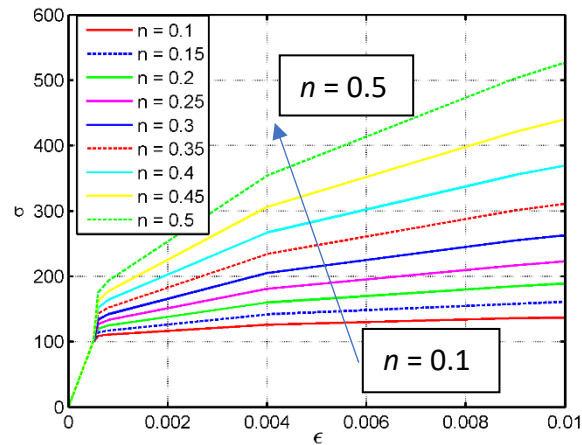
Fig 4.2: Stress vs strain for $E / S_Y = 2000$

In the Fig. 4.3, The effect of hardening exponent on the contact pressure area relation has analyzed. After analyzing the plot, an average error of 0.0001% was calculated for the hardening exponent ranging from $n = 0.1$- 0.5 because all the plots in this range coincided with each other. Since $\Delta <$ Δ_c it has no hardening effect for $E/S_Y = 20$ due to elastic nature. On the other hand, an average error of 0.0001% was calculated between the plots for $n = 0.01$ and 0.001. From the Fig. 4.3, we can conclude that there is no significant hardening effect. Fig. 4.3 is showing dimensionless contact pressure area relation with the hardening effect for $E/S_Y = 20$.

From the analysis of the effect of hardening for $E/S_Y = 200$ (Fig. 4.4) it has been found that with the increase in the hardening exponent value from $n = 0.1$ to 0.5 more pressure is required for complete contact to occur. Additionally, an average difference of 0.34% was calculated between the plots for $n = 0.01$ and 0.001. From the Fig. 4.4, we can conclude that below $n = 0.01$ there is no significant hardening effect. Fig. 4.4 is showing the dimensionless contact pressure area relation with the hardening effect for $E/S_Y = 200$. From Fig. 4.5, it has been found that the higher the value of hardening exponent the more pressure is required for complete contact to occur. An average difference of 0.15% was calculated between the plots for hardening exponents of $n = 0.001$ and $n = 0.01$, which means that below $n = 0.01$, there is no significant hardening effect for $E/S_Y = 2000$. In addition to this, a significant amount of hardening effect can be seen for the hardening exponents ranging from $n = 0.1$-0.5 for $E/S_Y = 2000$. The results obtained from power law hardening were also compared with bilinear Hardening for the same parameters.
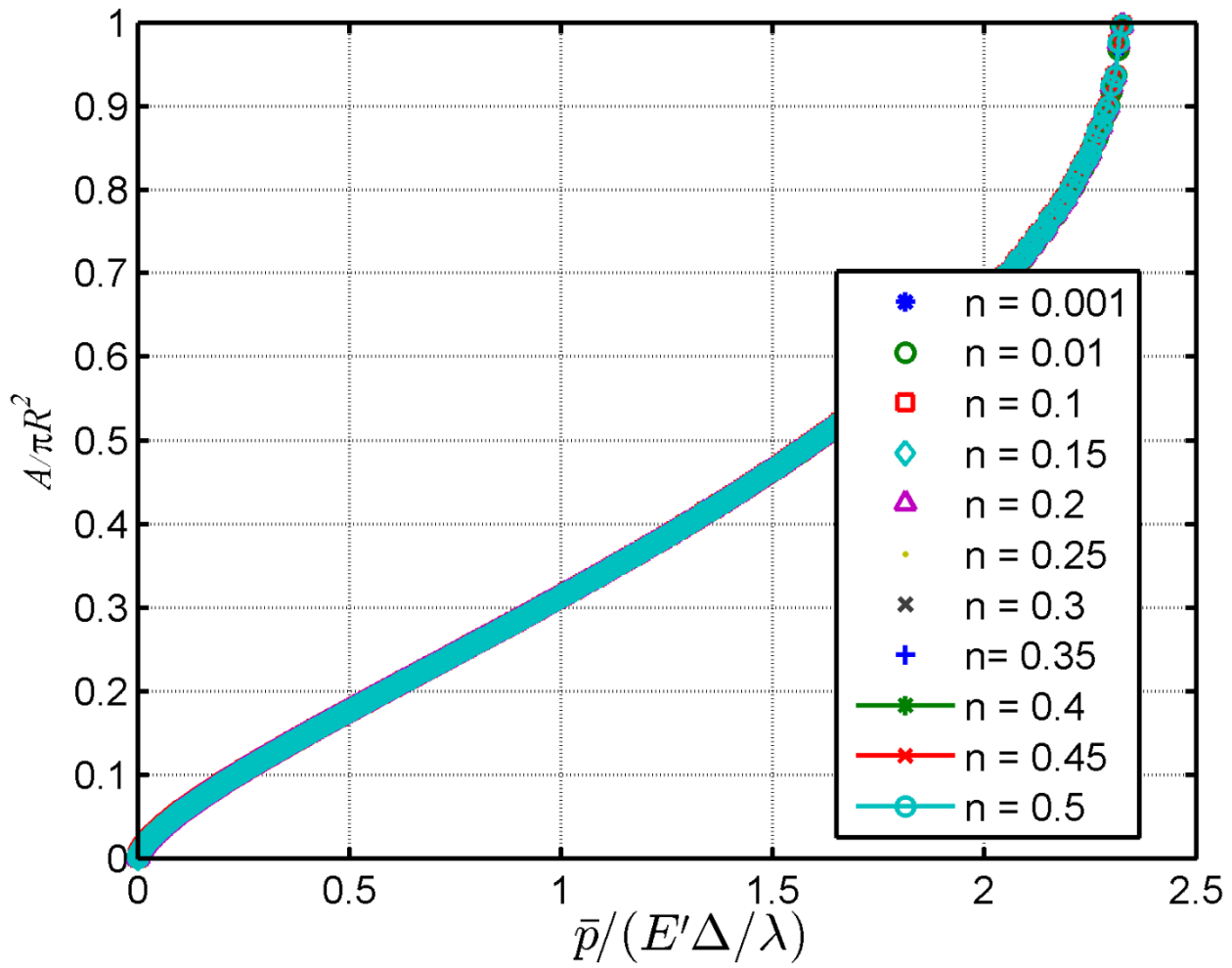
Fig. 4.3: Dimensionless contact pressure area relation with the hardening effect for $E/S_Y = 20$, $\Delta = 0.005$ *mm*
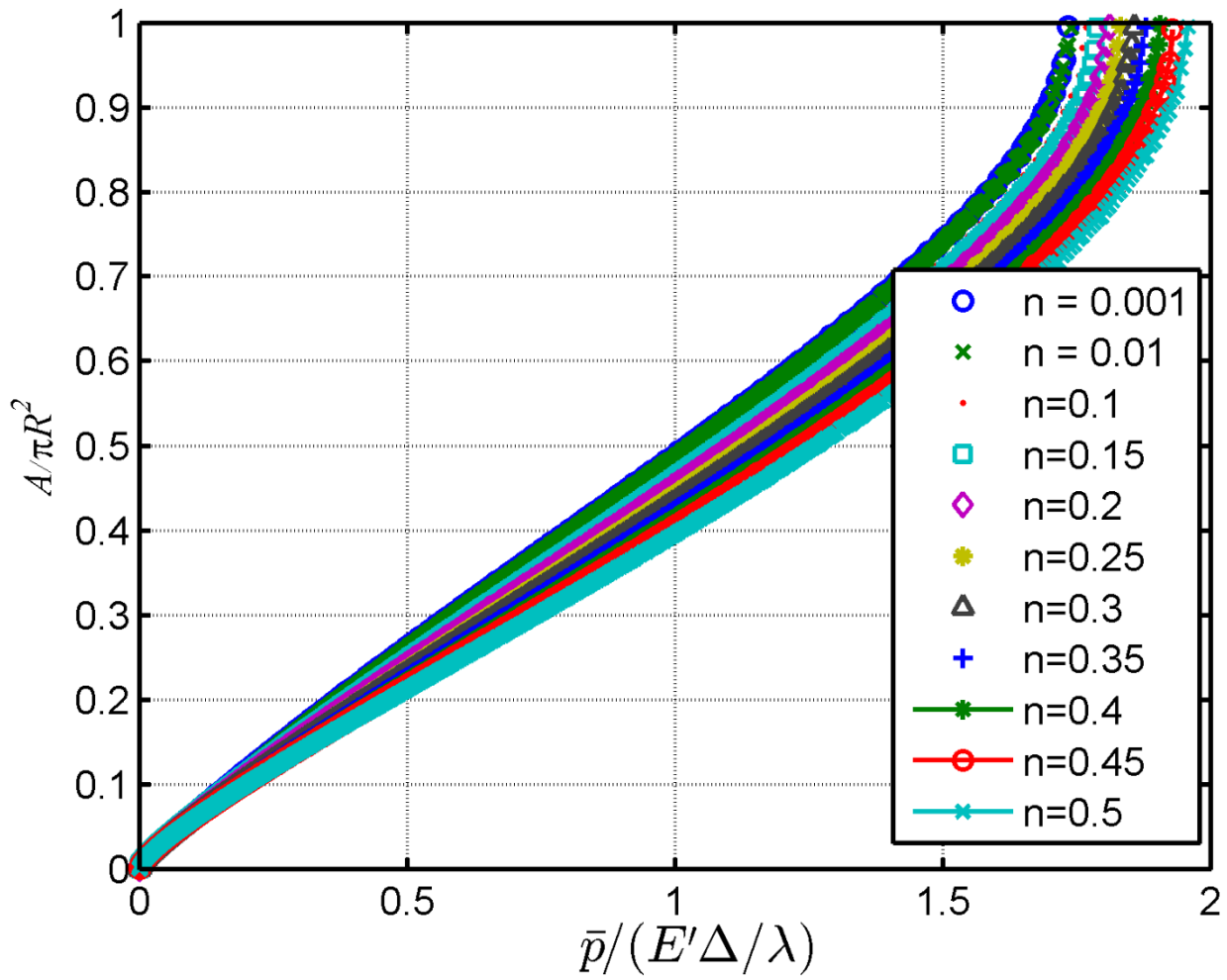
Fig. 4.4: Dimensionless contact pressure area relation with the hardening effect for $E/S_Y = 200$, $\Delta = 0.005$ *mm*
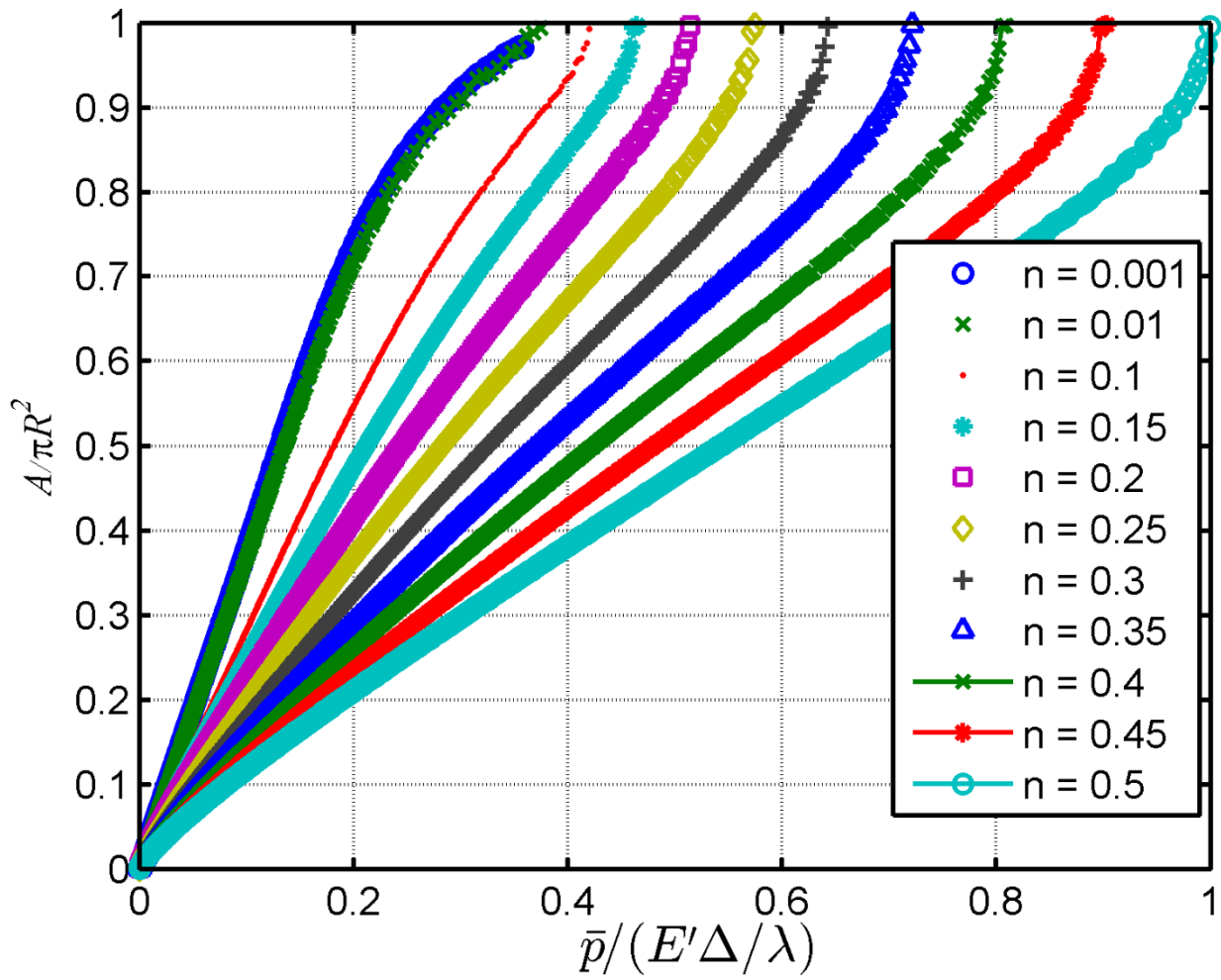
Fig. 4.5: Dimensionless contact pressure area relation with the hardening effect for $E/S_Y = 2000$, $\Delta = 0.005\ mm$
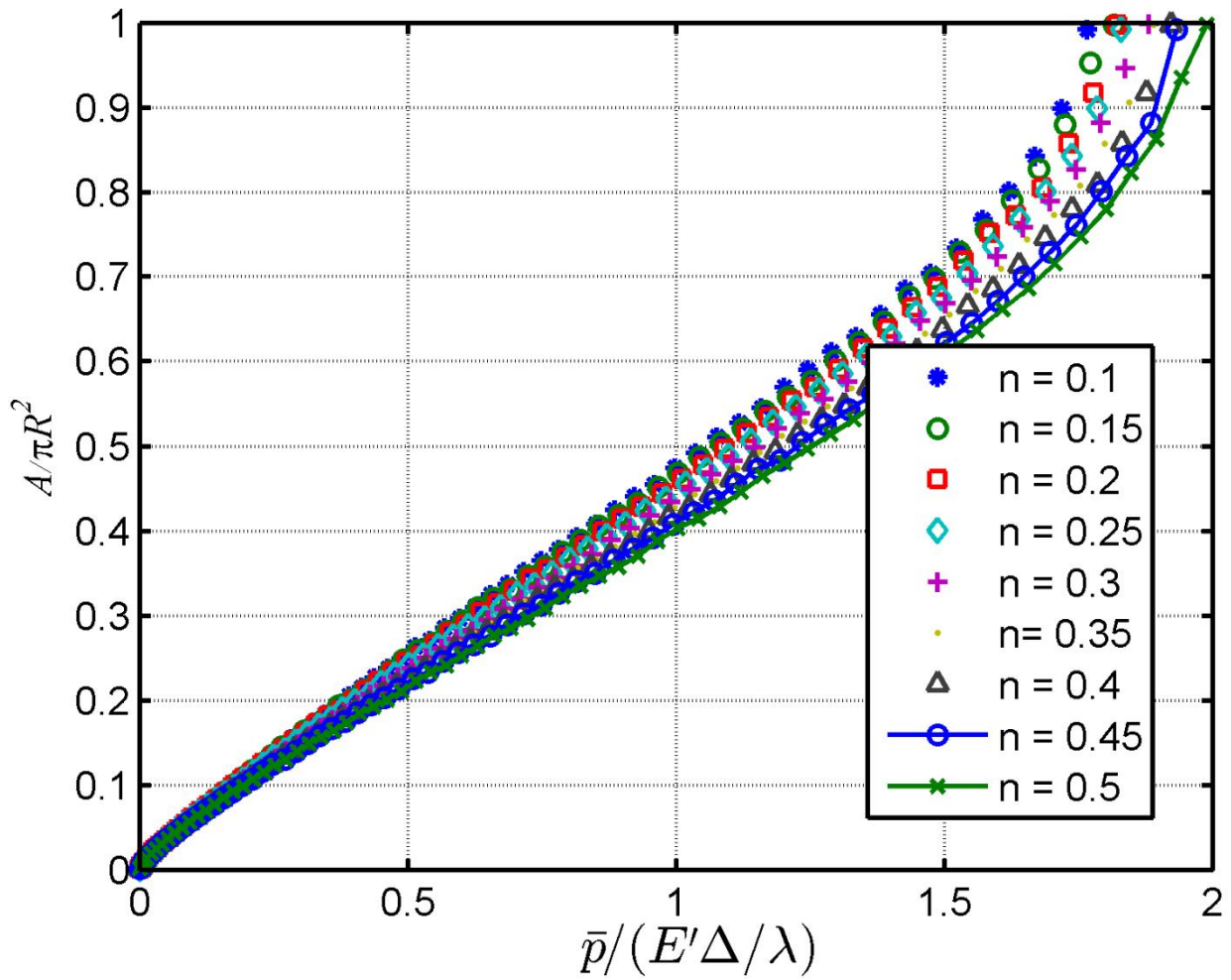
Fig. 4.6: Dimensionless contact pressure area relation with the hardening effect for $E/S_Y = 2000$, $\Delta= 0.0005$ *mm*

Constant value of $\Delta = 0.005$ mm, $\lambda = 1$ mm, $L_2 = 1.2$ mm, $E= 200\ GPa$ were used for this portion of the analysis. The average pressure, P^*_{EP-H}, that causes complete contact is extracted (section 3.4) from the finite element model data for each modeled case. This value corresponds to the average pressure when the area ratio, $A_{FEM}/_{\pi R^2} = 1$. At this stage complete contact occurs between the rigid flat and sinusoidal surface. The average pressure required for complete contact are given in Table 4.1, 4.2, 4.3, 4.4 respectively for each $E/_{S_Y}$. von Mises stress distribution for one of the case is shown in Fig. 4.11.
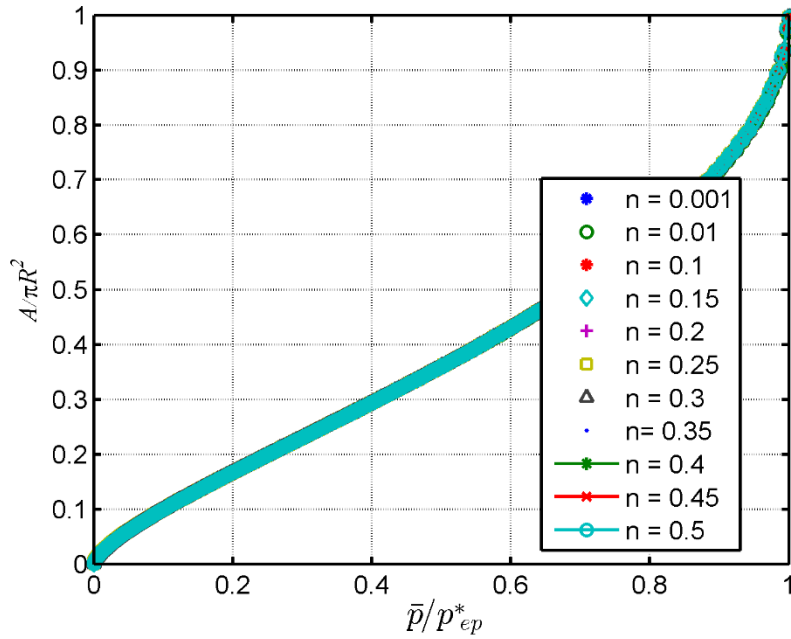
Fig. 4.7: Normalized contact pressure area for $E/_{S_Y} = 20$, $\Delta= 0.005\ mm$

42
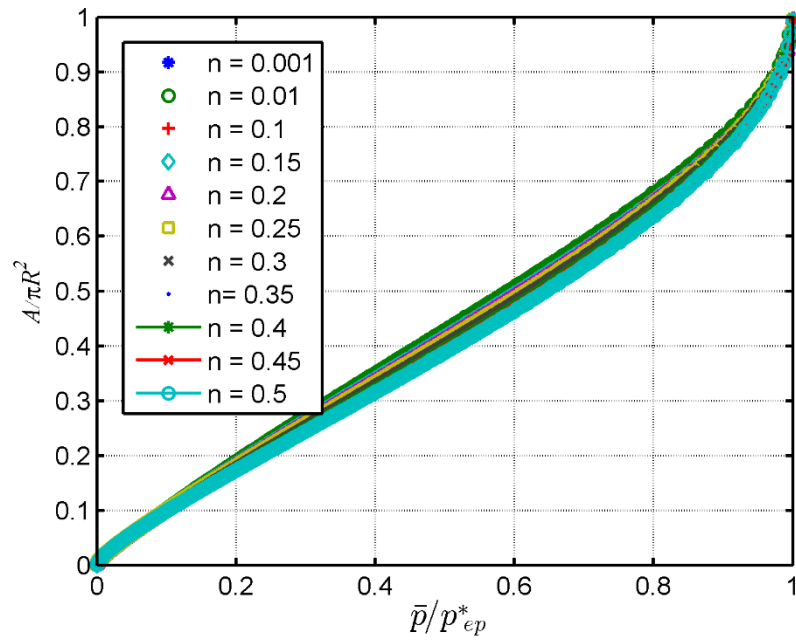
Fig. 4.8: Normalized contact pressure area for $E/S_Y = 200$, $\Delta = 0.005$ mm
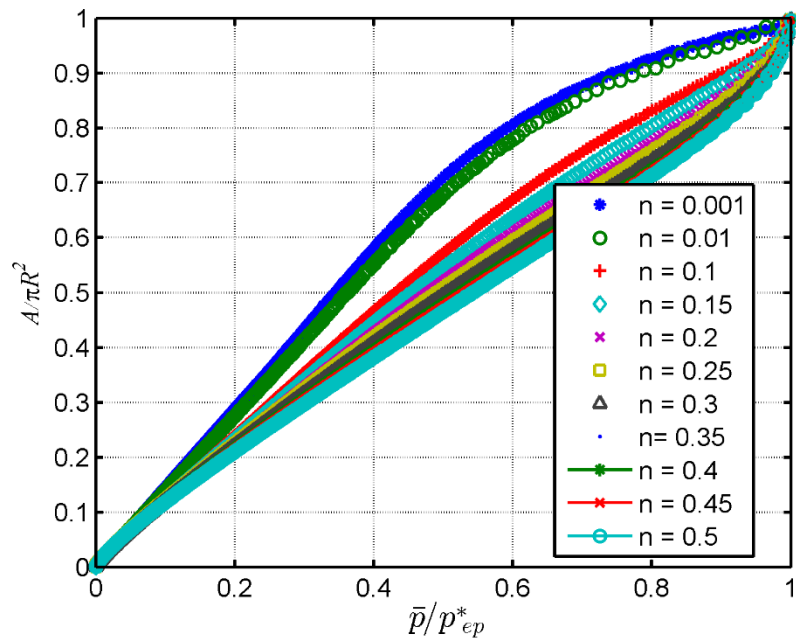
Fig. 4.9: Normalized contact pressure area for $E/S_Y = 2000$, $\Delta = 0.005$ mm

43
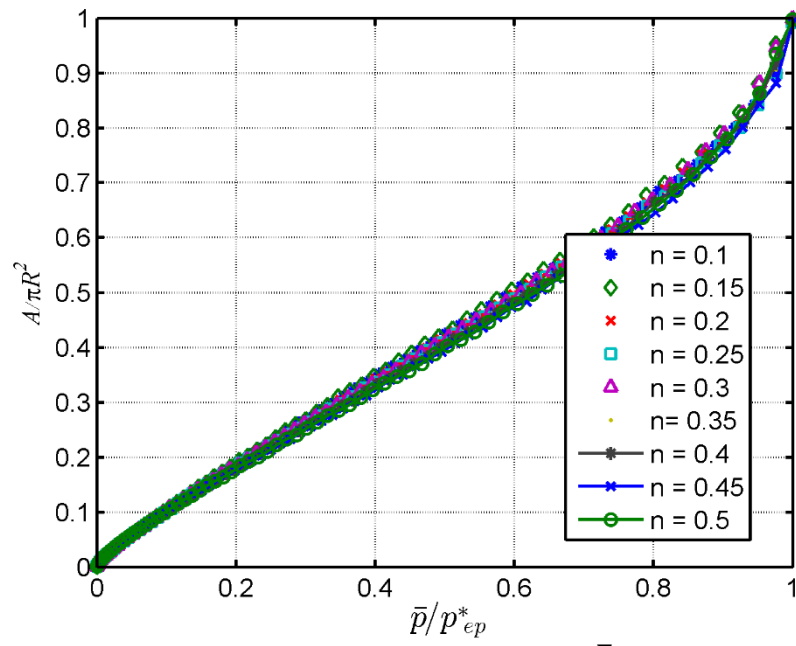
Fig. 4.10: Normalized contact pressure area for $E/S_Y = 2000$, $\Delta = 0.0005$ *mm*

Table 4.1: Average pressure required for complete contact for $E/S_Y = 20$, $\Delta = 0.005$ mm

n	P^*_{EP-H}
0.001	*2.606 GPa*
0.01	*2.606 GPa*
0.1	*2.609 GPa*
0.15	*2.609 GPa*
0.2	*2.609 GPa*
0.25	*2.609 GPa*
0.3	*2.609 GPa*
0.35	*2.609 GPa*
0.4	*2.609 GPa*
0.45	*2.609 GPa*
0.5	*2.609 GPa*

Table 4.2: Average pressure required for complete contact for $E/S_Y = 200$, $\Delta = 0.005$ mm

n	P_{EP-H}^*
0.001	*1.945 GPa*
0.01	*1.951 GPa*
0.1	*1.983 GPa*
0.15	*2.006 GPa*
0.2	*2.033 GPa*
0.25	*2.056 GPa*
0.3	*2.084 GPa*
0.35	*2.108 GPa*
0.4	*2.138 GPa*
0.45	*2.164 GPa*
0.5	*2.197 GPa*

Table 4.3: Average pressure required for complete contact for $E/S_Y = 2000$, $\Delta = 0.005$ mm

n	P^*_{EP-H}
0.001	0.420 GPa
0.01	0.427 GPa
0.1	0.471 GPa
0.15	0.521 GPa
0.2	0.577 GPa
0.25	0.645 GPa
0.3	0.721 GPa
0.35	0.809 GPa
0.4	0.907 GPa
0.45	1.013 GPa
0.5	1.121 GPa

Table 4.4: Average pressure required for complete contact for $E/S_Y = 2000$, $\Delta = 0.0005$ mm

n	P^*_{EP-H}
0.1	*0.198 GPa*
0.15	*0.203 GPa*
0.2	*0.204 GPa*
0.25	*0.205 GPa*
0.3	*0.211 GPa*
0.35	*0.212 GPa*
0.4	*0.215 GPa*
0.45	*0.216 GPa*
0.5	*0.223 GPa*
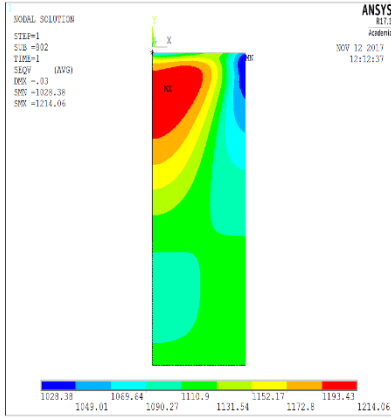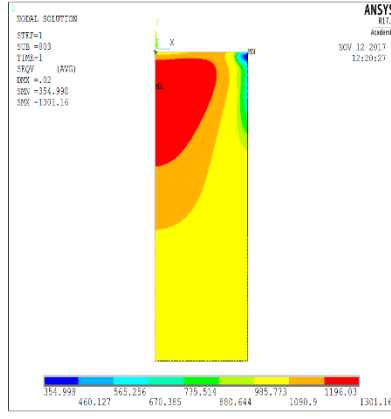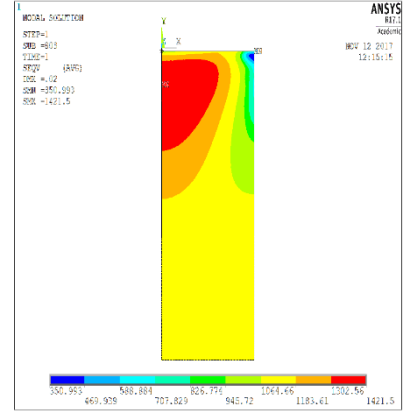
A: $n = 0.1$ B: $n = 0.15$ C: $n = 0.2$
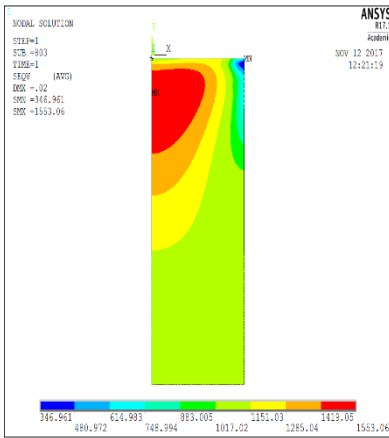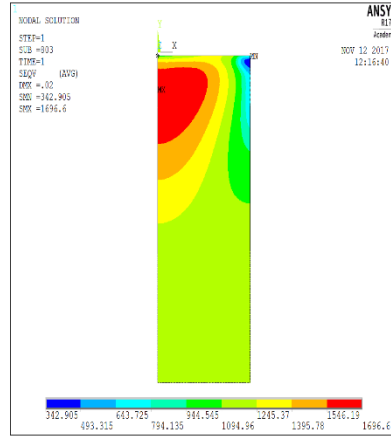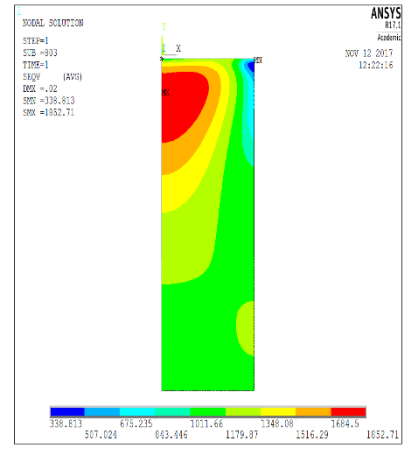
D: $n = 0.25$ E: $n = 0.3$ F: $n = 0.35$
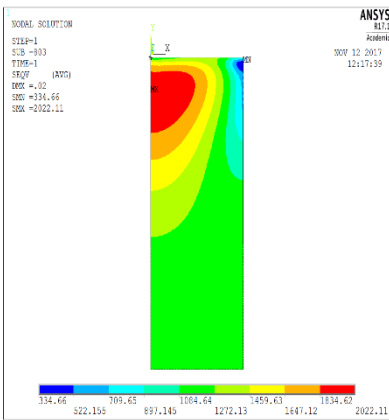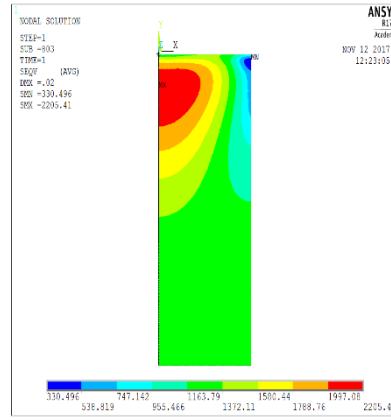
G: $n = 0.4$ H: $n = 0.45$

Fig. 4.11: von Mises stress *(N/mm^2)* of n = 0.1, 0.15, 0.2, 0.25, 0.3, 0.35, 0.4, 0.45 for E/S_Y = 200, Δ = 0.005 mm respectively.

Table 4.5: Maximum von Mises stress values for $E/S_Y = 200$, $\Delta = 0.005$ mm

Hardening exponent (*n*)	von Mises Stress (*GPa*)
0.1	1.214
0.15	1.301
0.2	1.421
0.25	1.553
0.3	1.696
0.35	1.852
0.4	2.022
0.45	2.205
0.5	2.643

Table 4.6: Maximum von Mises stress values for $E/S_Y = 2000$, $\Delta = 0.005$ mm

Hardening exponent (*n*)	von Mises Stress (*GPa*)
0.1	0.156
0.15	0.198
0.2	0.236
0.25	0.295
0.3	0.346
0.35	0.418
0.4	0.502
0.45	0.603
0.5	0.732

Table 4.7: Maximum von Mises stress values for $E/S_Y = 2000$, $\Delta = 0.0005$ mm

Hardening exponent (*n*)	von Mises Stress (*GPa*)
0.1	0.139
0.15	0.165
0.2	0.195
0.25	0.230
0.3	0.272
0.35	0.321
0.4	0.379
0.45	0.448
0.5	0.529

4.3   Bi-Linear Isotropic Hardening

In order to compare the results obtained from power law hardening with the bi-linear isotropic hardening a number of simulations were carried out. In this section, the material is being modeled as an elastic-plastic material with bilinear isotropic hardening. Two different values of E/S_Y = (200, 2000) were considered for a constant value of amplitude (Δ = 0.005 mm) and wavelength (λ = 1 mm) was used throughout the calculation. Then, the analysis was done for a fixed value of Young's modulus (E = 200 GPa) and for four different values of tangential modulus ($E_T = 1\%E, 2\%E, 5\%E, 10\%E$). Finally, for each E/S_Y ratio all the results were plotted on a single graph for different values of tangential modulus. The results obtained from FEM are discussed in next section. The stress strain relationship for bilinear hardening are as follow:
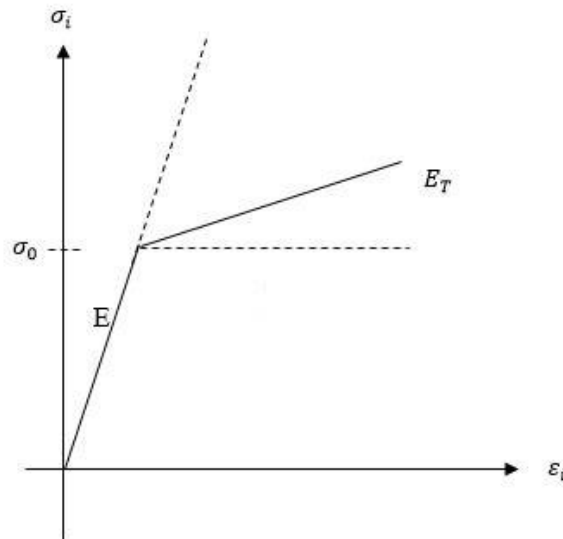
Fig. 4.12: Stress-strain curve for Bilinear Isotropic Hardening
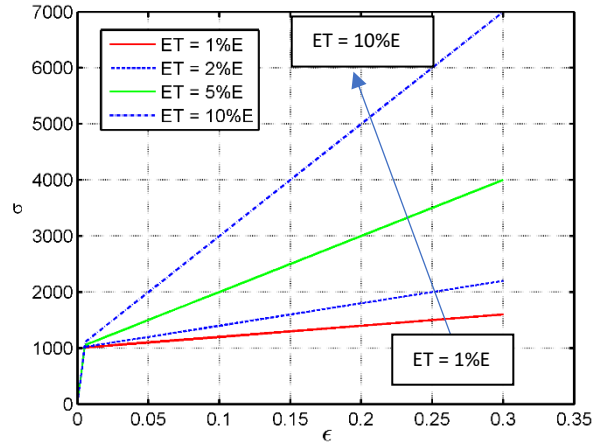
Fig 4.13: Stress vs strain for $E/S_Y = 200$
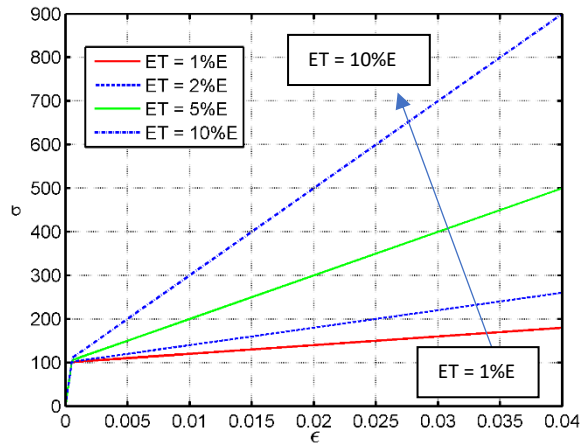
Fig 4.14: Stress vs strain for $E/S_Y = 2000$

In Fig 4.13 and Fig 4.14, The stress strain relationship for bilinear hardening is analyzed for four different values of tangent modulus and two different E/S_Y . The region below yield strength is the elastic region whereas the region after the yield strength is the plastic region which is described by the slope of tangent modulus. The dimensionless contact pressure area relation for bilinear hardening are discussed below.
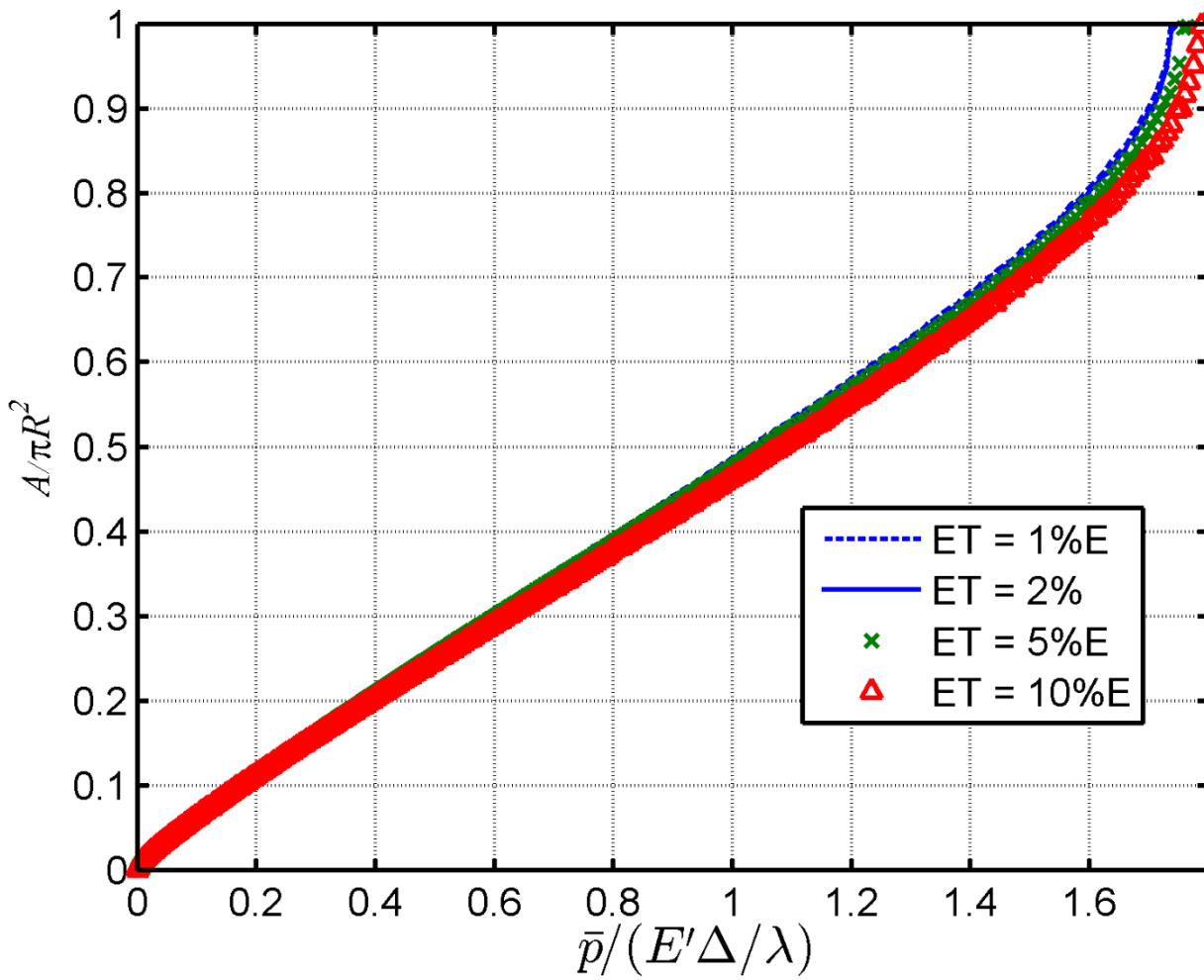
Fig. 4.15: Dimensionless contact pressure area relation with the hardening effect for $E/S_Y = 200, \Delta = 0.005 \ mm$
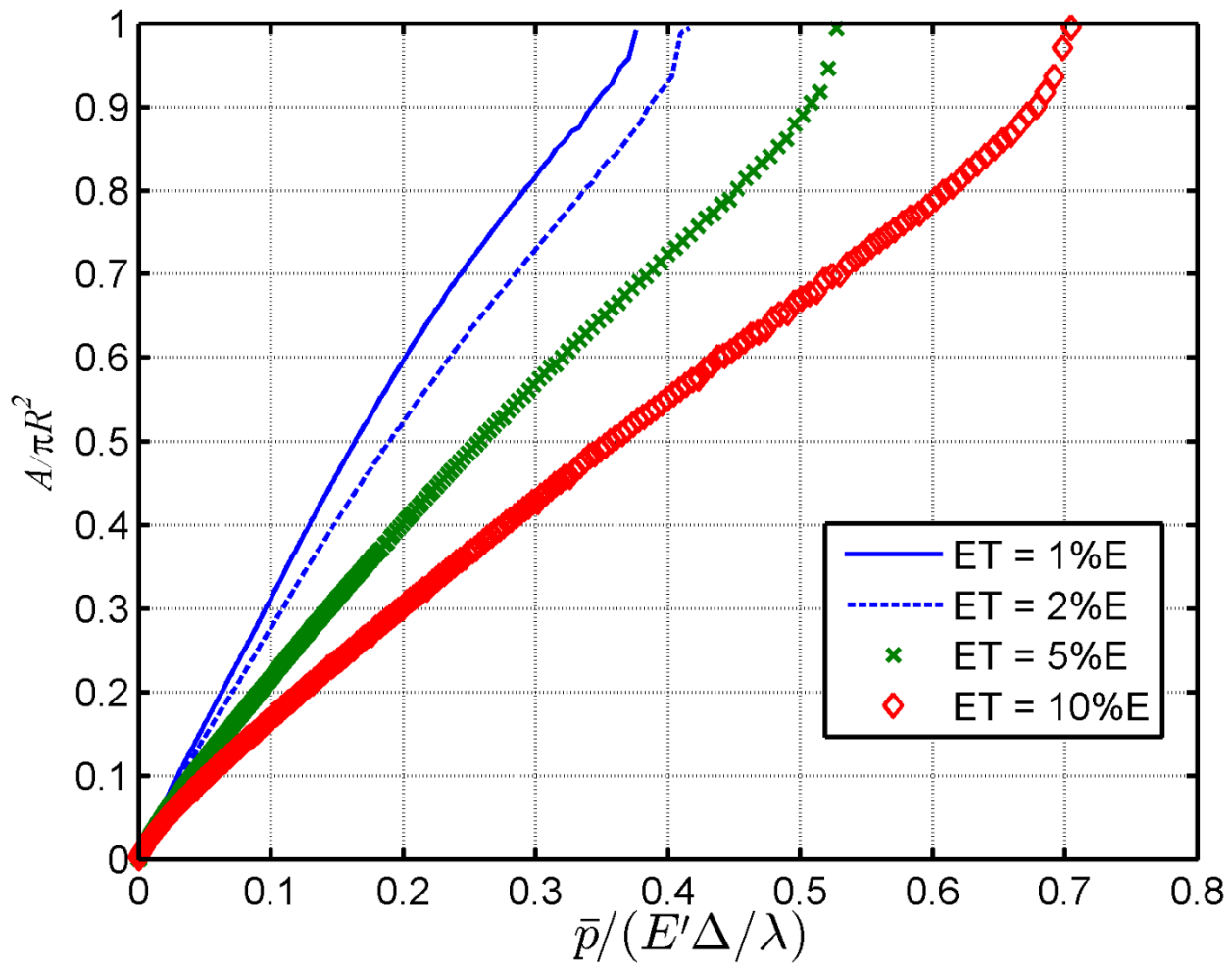
Fig. 4.16: Dimensionless contact pressure area relation with the hardening effect for ${E}/{S_Y} = 2000, \Delta = 0.005$ *mm*
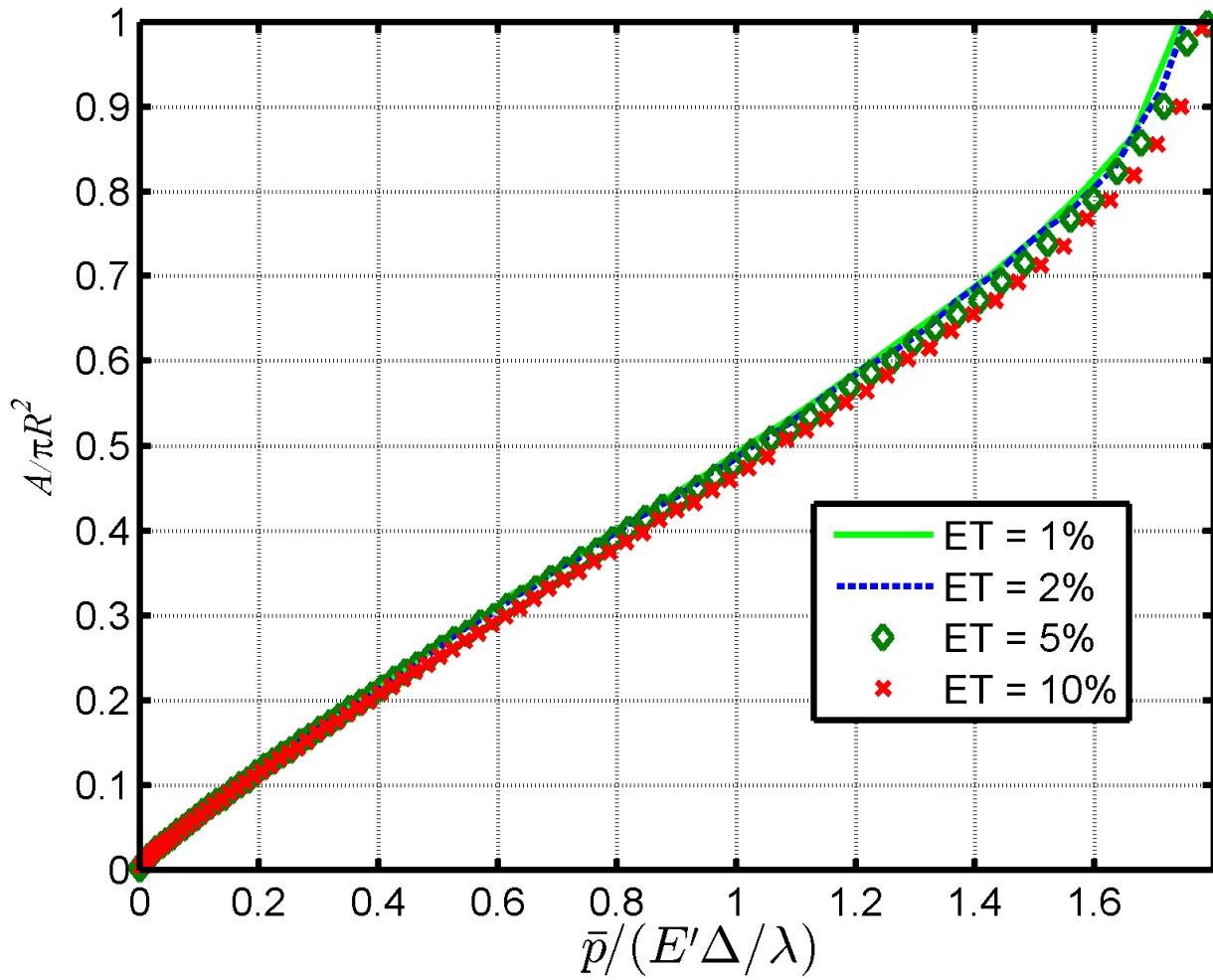
Fig. 4.17: Dimensionless contact pressure area relation with the hardening effect for $E/S_Y = 2000$, $\Delta = 0.0005$ *mm*

In Fig. 4.15, The effect of tangential modulus, E_T, on the contact pressure area relation is analyzed. After analyzing the plot, it can be concluded that no significant hardening effect is observed between $E_T = 1\%E \ and \ 2\%E$ for $E/S_Y = 200, \ \Delta= 0.005$ because an average error of 0.3% was calculated for these two cases. In Fig. 4.16, A significant amount of the hardening effect was observed which means more pressure is required with the increase in tangential modulus to achieve the complete contact between the sinusoidal surface and the rigid flat. In Fig. 4.17, no significant amount of hardening was observed as all the plots are very close to each other. Kogut and Etsion [34] showed that for E_t <2%E hardening does not have significant effect. However, in the current work it was found that hardening has significant effect for E_t <2%E. Table 4.8, 4.9, 4.10 are showing the average pressure values required for complete contact for the bi -Linear isotropic hardening model.
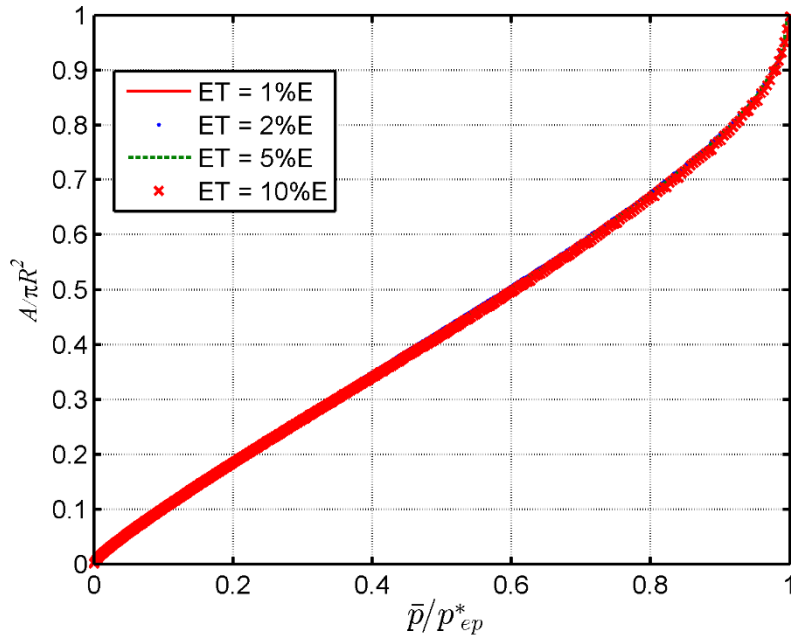
Fig. 4.18: Normalized contact pressure area for $E/S_Y = 200, \Delta= 0.005 \ mm$
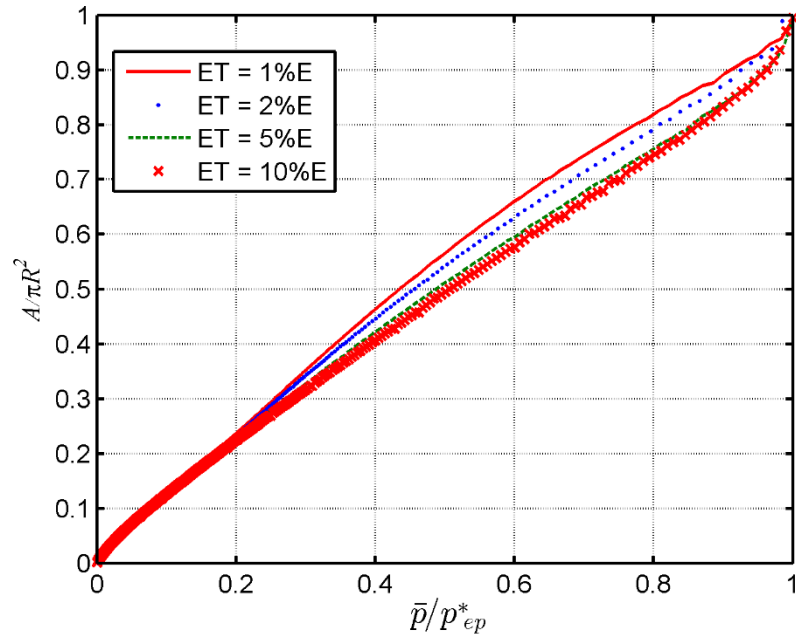
Fig. 4.19: Normalized contact pressure area for $E/S_Y = 2000$, $\Delta = 0.005$ *mm*
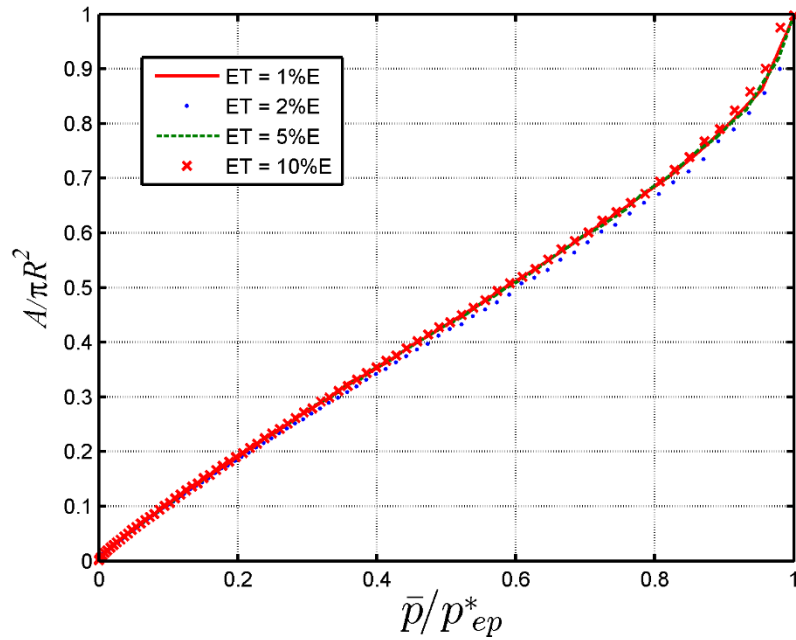
Fig. 4.20: Normalized contact pressure area for $E/S_Y = 2000$, $\Delta = 0.0005$ *mm*

Table 4.8: Average pressure required for complete contact for $E/S_Y = 200$, $\Delta = 0.005$ mm

E_T	P^*_{EP-H}
1%	1.948 GPa
2%	1.959 GPa
5%	1.981 GPa
10%	2.007 GPa

Table 4.9: Average pressure required for complete contact for $E/S_Y = 2000$, $\Delta = 0.005$ mm

E_T	P^*_{EP-H}
1%	0.422 GPa
2%	0.466 GPa
5%	0.591 GPa
10%	0.790 GPa

Table 4.10: Average pressure required for complete contact for $E/S_Y = 2000$, $\Delta = 0.0005$ mm

E_T	P^*_{EP-H}
1%	0.195 GPa
2%	0.196 GPa
5%	0.200 GPa
10%	0.202 GPa

However, the current work finds that it is possible to account for power law and bilinear hardening via an effective yield strength, S_E. Following the definition of power law and bilinear hardening, the approximate prediction of the effective yield strength is found by fitting to the finite element data for the complete contact pressure cases. The expression for S_E for both the hardening is given by:

For power law hardening:

$$S_E = S_Y + E \cdot x^{(a \cdot x + b)} \cdot y^{(c \cdot x + d)} \tag{4.2}$$

Where S_Y is the yield strength, E is the elastic modulus, x is Δ/λ, y is the hardening exponent, n, and a, b, c, d, are the constants which is given below:

Table 4.11: Constants of S_E for power law hardening

Δ/λ	E/S_Y	a	b	c	d
0.005	200	-26.98	1.149	-595.1	4.071
0.005	2000	-1.486	0.9778	283.9	0.6983
0.0005	2000	-1.486	0.9778	283.9	0.6983

For bilinear hardening:

The same equation 4.2 was used for calculating the effective yield strength. Where x is Δ/λ, and y is given by E_T/E. The constant values are given in Table 4.12.

Table 4.12: Constants of S_E for Bilinear hardening

Δ/λ	E/S_Y	a	b	c	d
0.005	200	-0.09	1	-9.51E+03	47.99
0.005	2000	-101	1.203	276.2	0.2346
0.0005	2000	-101	1.203	276.2	0.2346
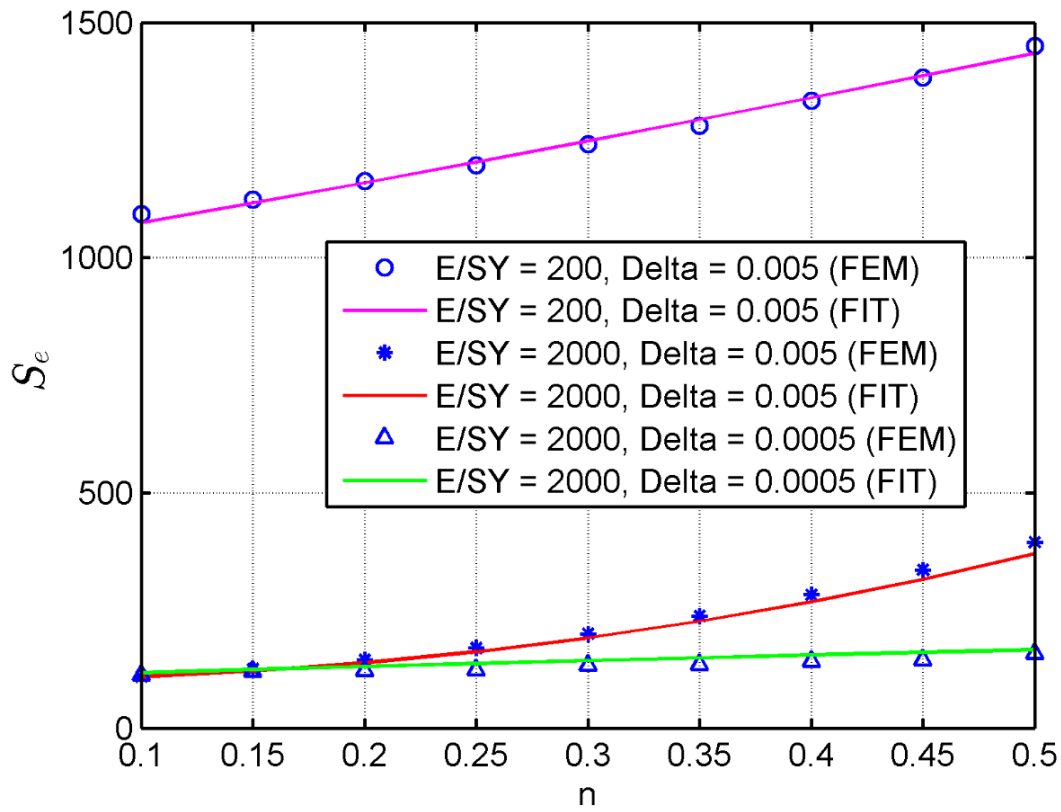
Fig. 4.21: S_E vs n
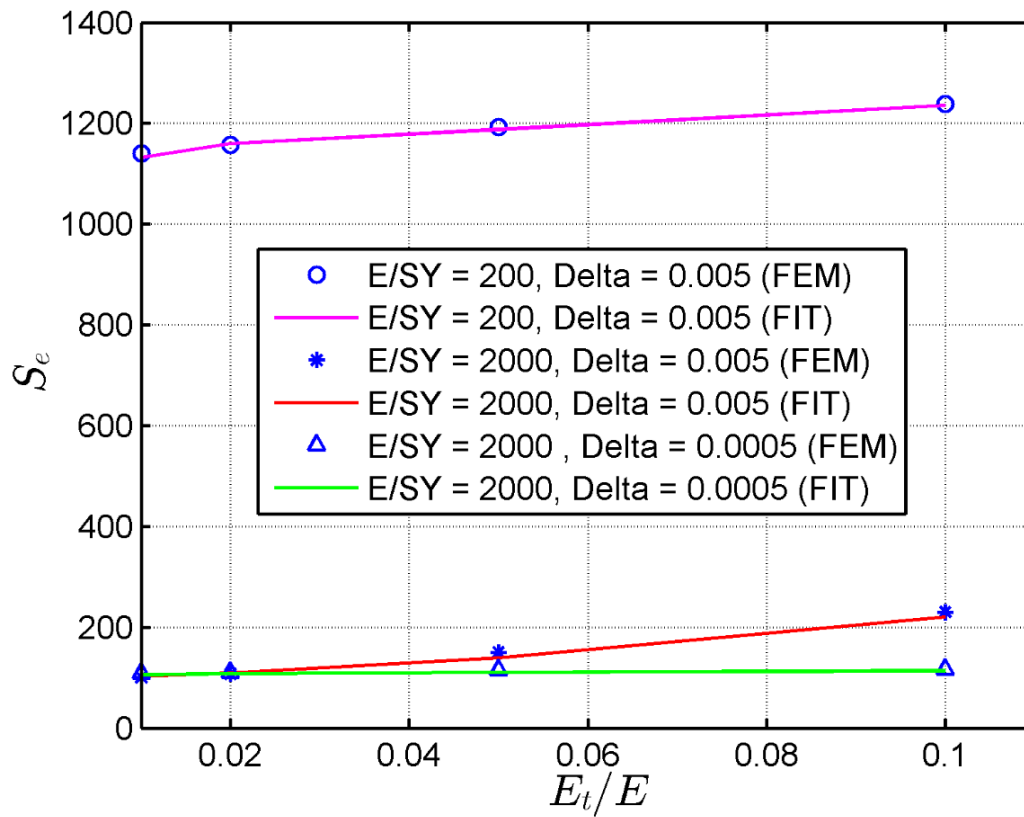
Fig. 4.22: S_E vs ${E_T}/{E}$.

4.4   Surface Separation Results for Power law and Bilinear Isotropic Hardening

Using the same material properties as in section 4.2 and 4.3, the average surface separation results for different ${E}/{S_Y}$ was observed. Fig 4.23, 4.24, 4.25, 4.26 is representing the plots for the FEM elasto-plastic results for average surface separation for different ${E}/{S_Y}$.
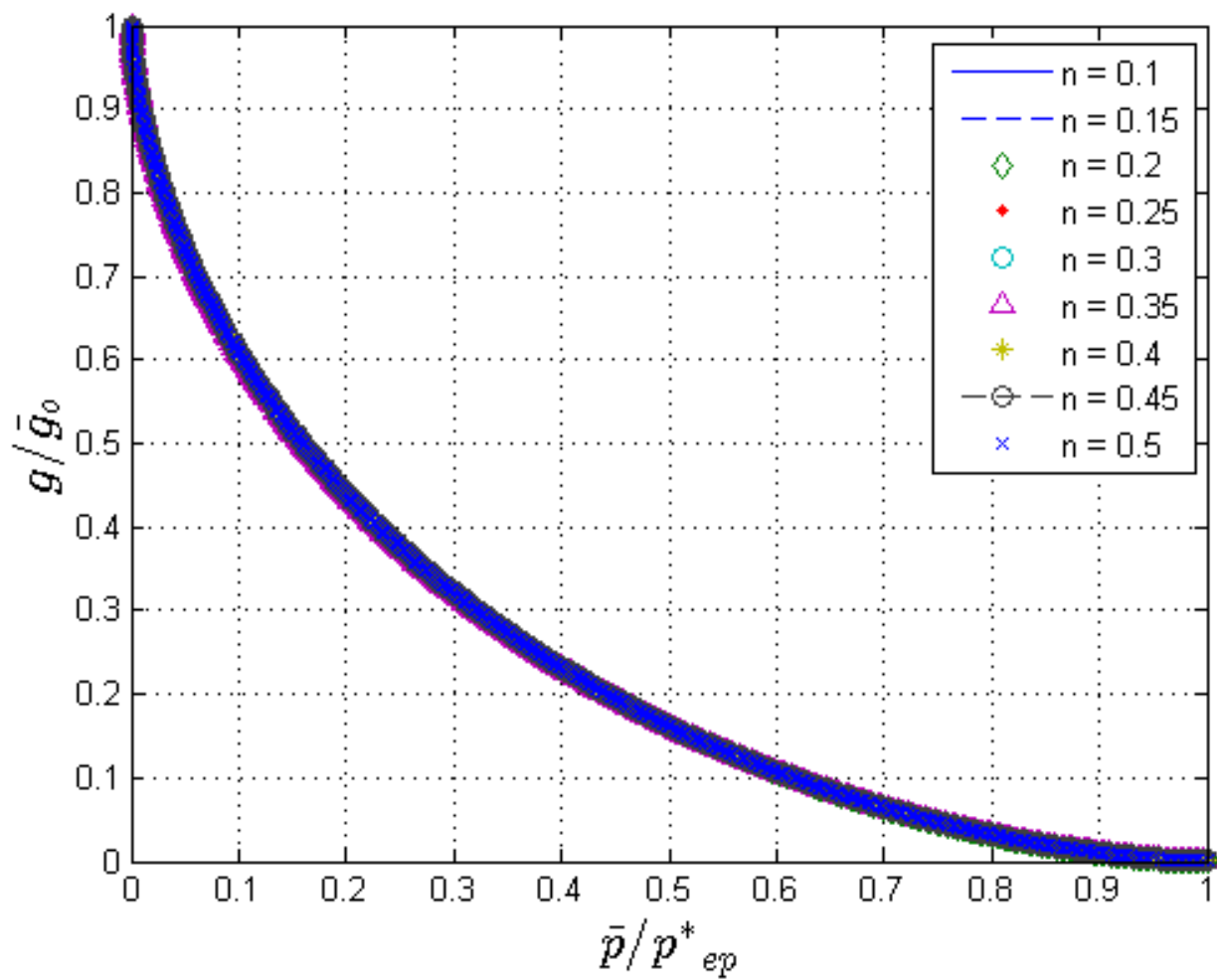
Fig 4.23: The FEM elastic-plastic results for average surface separation for $E/S_Y = 20$
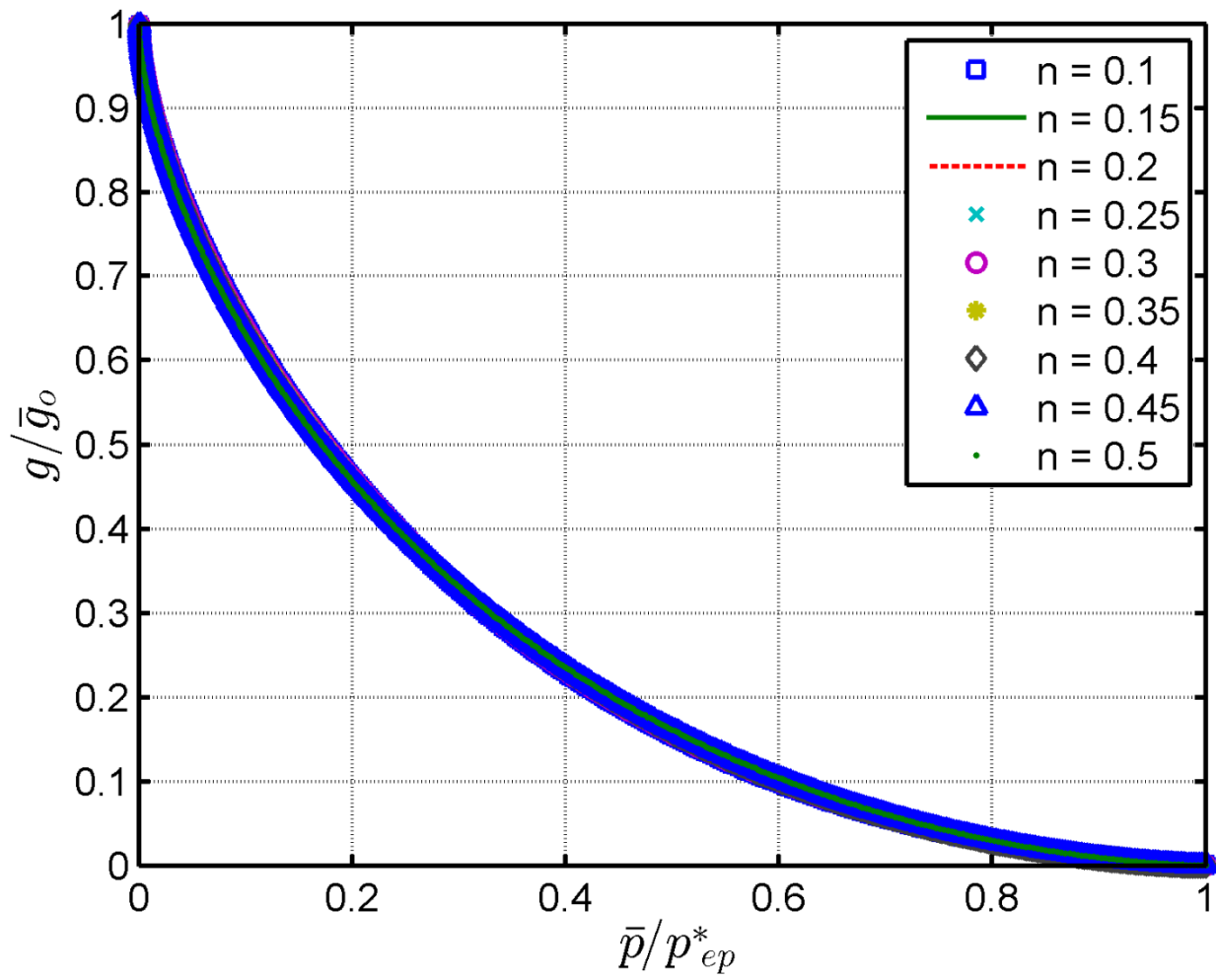
Fig. 4.24: The FEM elastic-plastic results for average surface separation for $E/S_Y = 200$
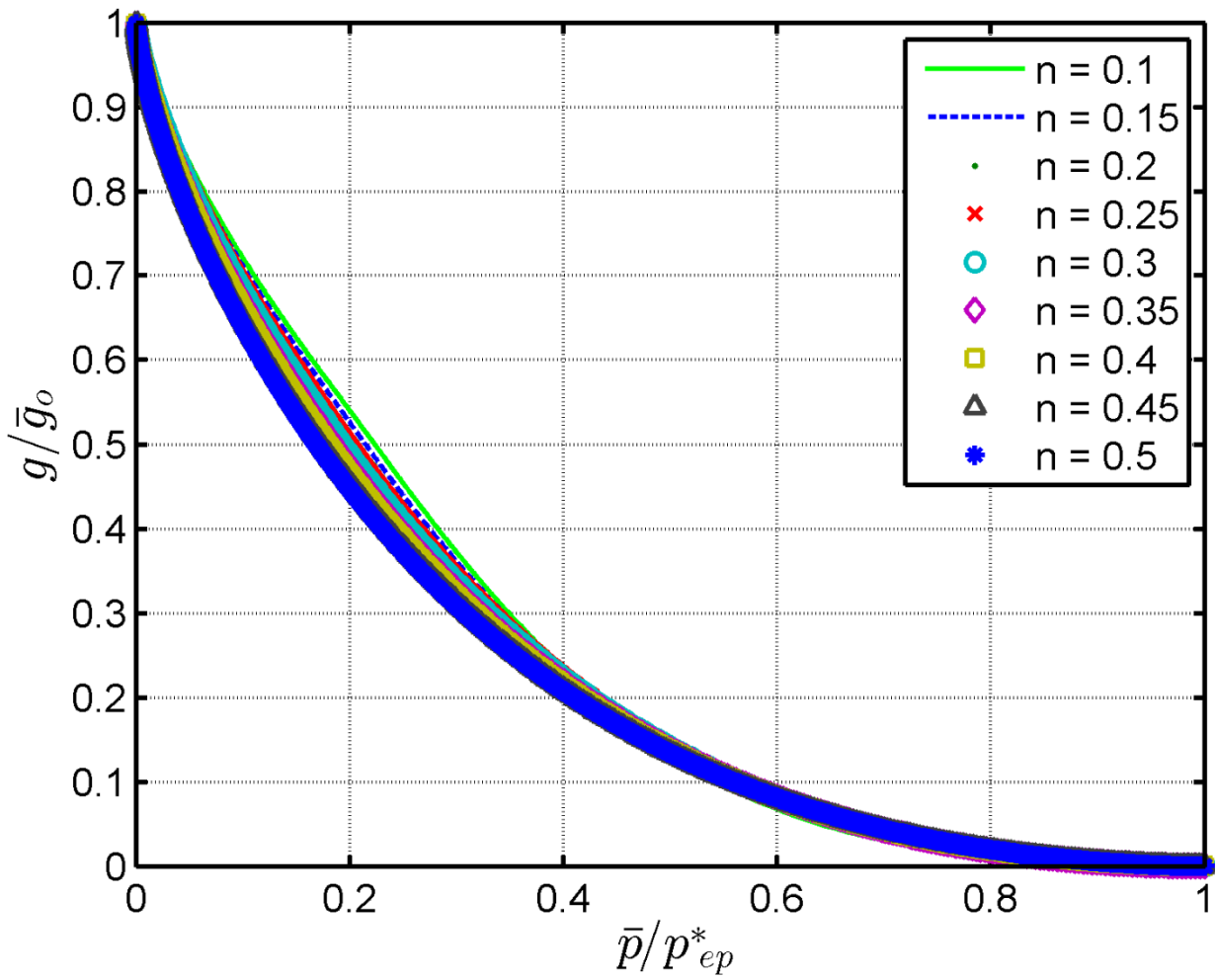
Fig 4.25: The FEM elastic-plastic results for average surface separation for $E/S_Y = 2000$
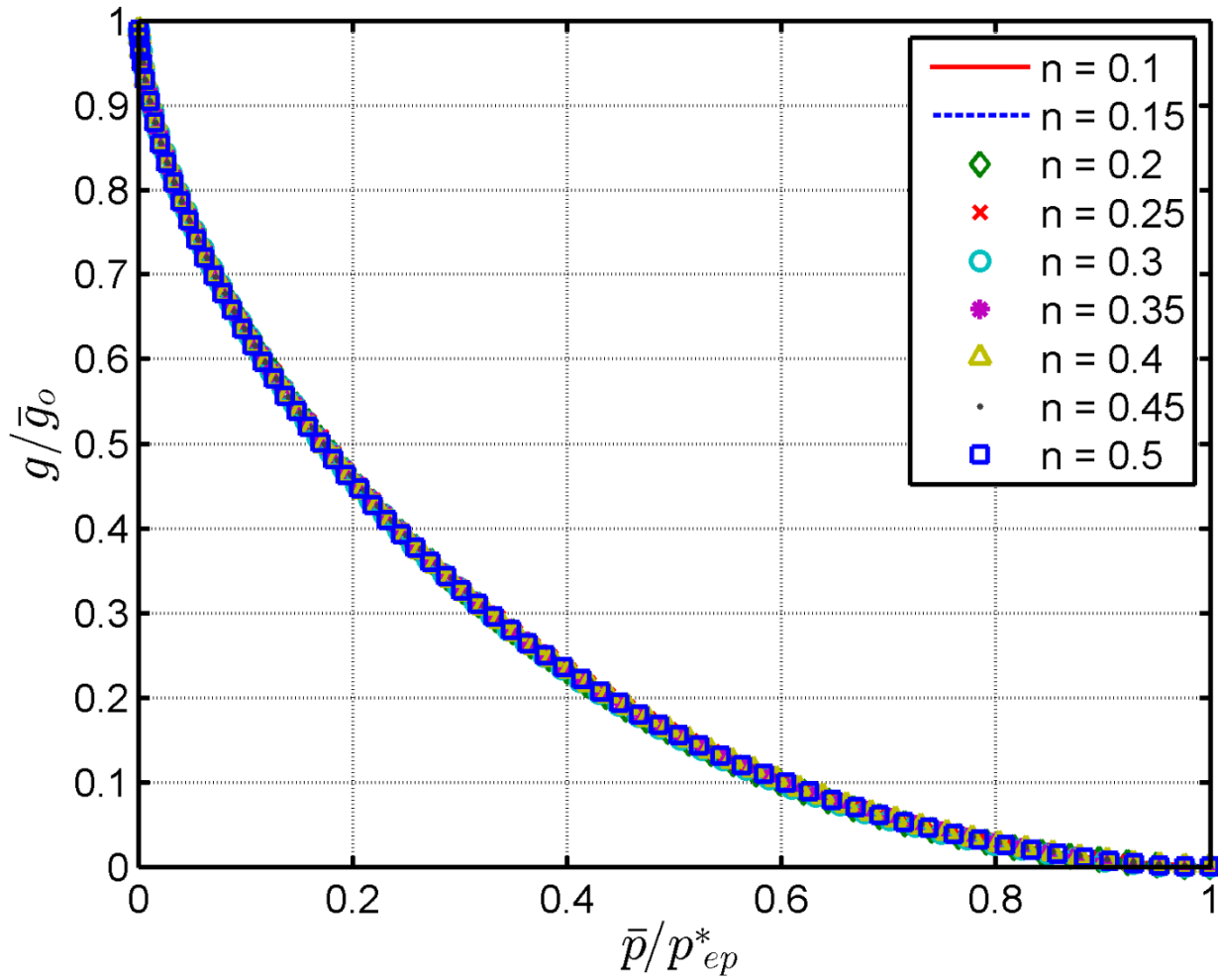
Fig 4.26: The FEM elastic-plastic results for average surface separation for $\frac{E}{S_Y} = 2000, \Delta = 0.0005mm$

From the plots above, no significant effect of hardening is observed as they are coinciding with each other. There is a little deviation in Fig 4.24 and Fig 4.25 but at the end it also converges. The results were normalized for better understanding of the plots. The plots of surface separation for

Bilinear Isotropic hardening are shown in next section. The expression used to normalize the average gap is as follow:

$$\overline{g_o} = \left(\frac{\frac{\pi \cdot \Delta \cdot \lambda^2}{4} + \frac{\Delta \cdot \lambda^2}{\pi}}{\pi \cdot \frac{\lambda^2}{4}} \right) \tag{4.3}$$
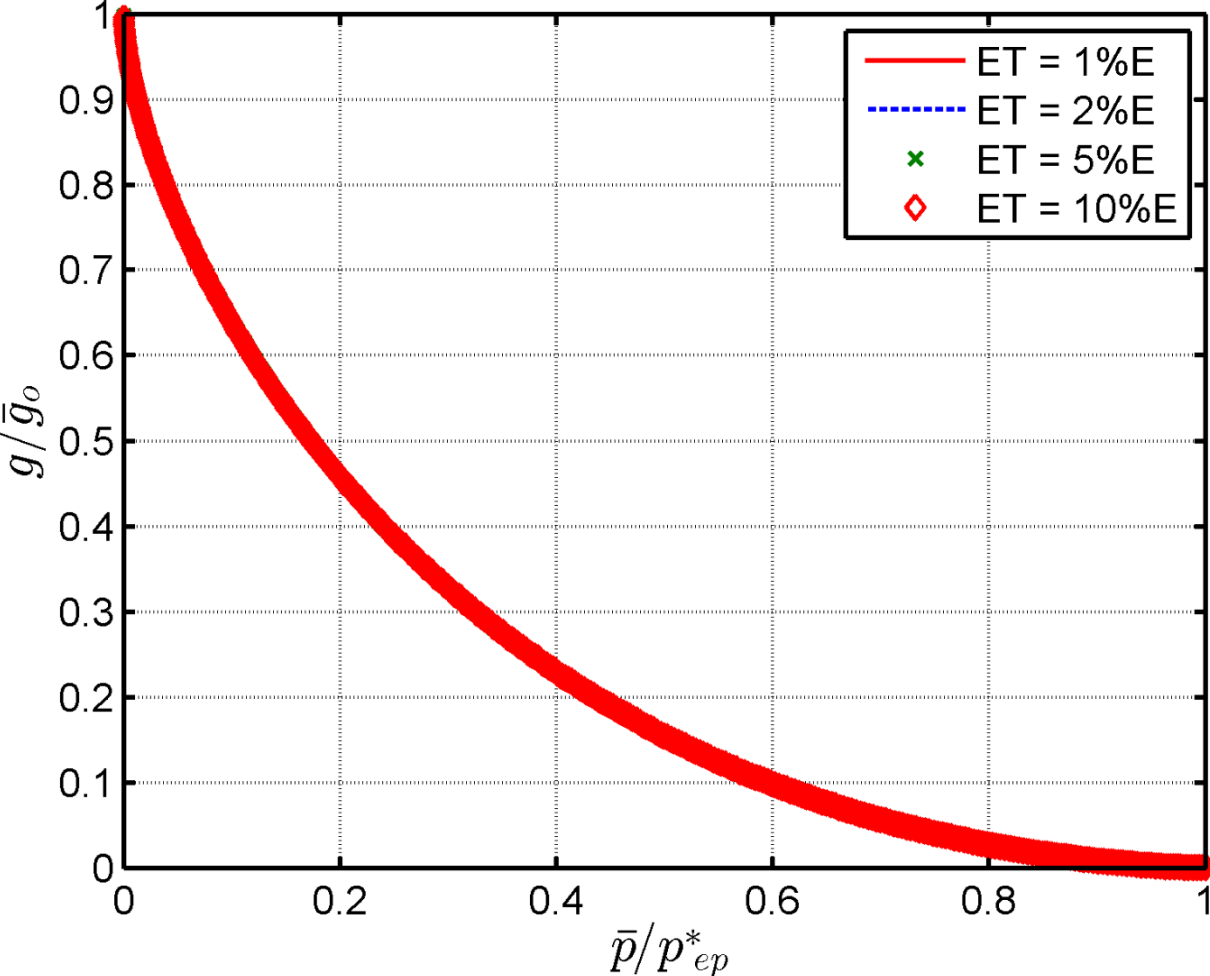
Fig 4.27: The FEM elasto-plastic results for average surface separation for $E/S_Y = 200$
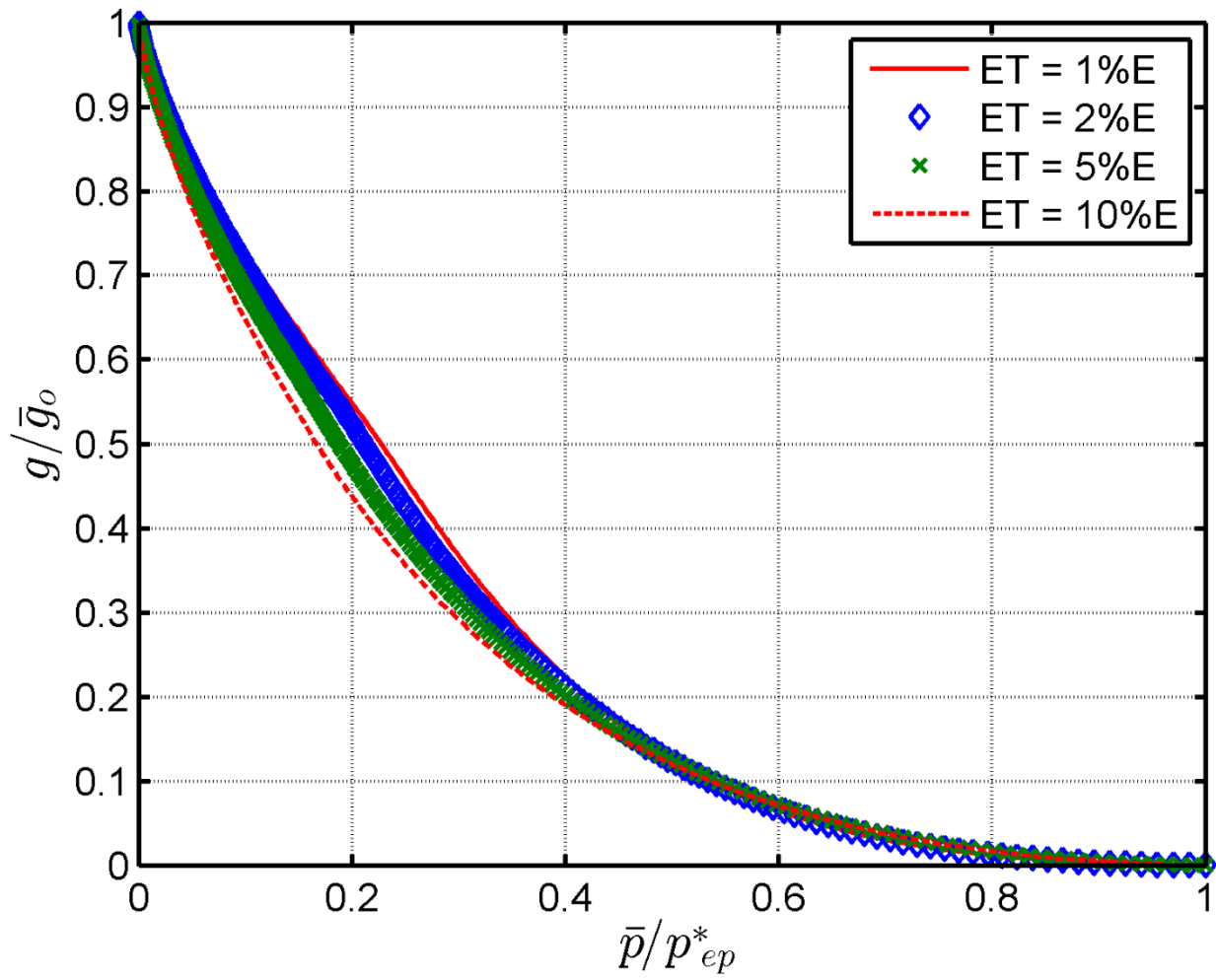
Fig 4.28: The FEM elasto-plastic results for average surface separation for $E/S_Y = 2000$
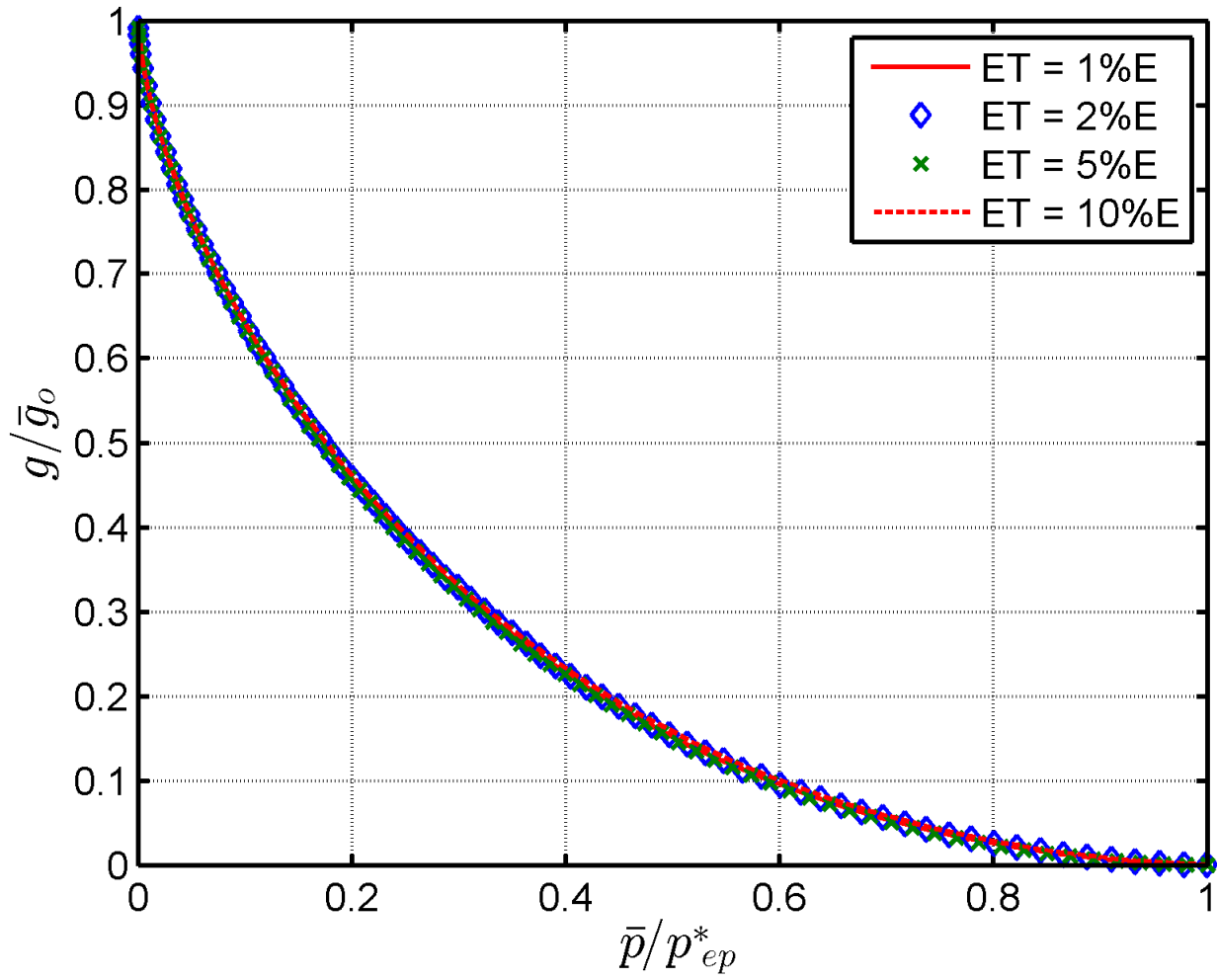
Fig 4.29: The FEM elasto-plastic results for average surface separation for $E/S_Y = 2000, \Delta = 0.0005mm$

Chapter 5

Conclusions

Rough surfaces are very common in the real world. From a microscopic point of view, interactions between rough surfaces are happening between peaks or asperities. In order to understand the real mechanisms behind the interaction between the asperities or rough surfaces, different types of methods have been developed for modelling rough surface contact.

In this work, the contact problem comprised of a strain hardening elastic plastic axisymmetric sinusoidal surface asperity and a rigid flat was analyzed and modelled using the finite element method. A numerical model was generated using the commercial finite element software ANSYS 17.1. The surface is modelled as an elastic plastic, nonlinear isotropic power law hardening solid. Since the nature of asperity is axisymmetric (Fig. 3.2), only the right half of the asperity (two dimensional) was taken into consideration.

This work also characterizes the pressure required to cause complete contact between the surfaces. Complete contact is defined as when there is no gap between the two surfaces in contact. In the end, the FEM model is used to produce equations which can be employed to approximately relate the area of contact to the contact pressure for elastic-plastic sinusoidal contact. The results obtained from power law hardening are also compared with the results obtained from bilinear hardening for $E_T = 1\% \, E, 2\% \, E, 5\% \, E, 10\% \, E$ in order to observe the possible change in trend for two different types of hardening. From the plots, it can be concluded that with the increase in

hardening more pressure is required for complete contact to occur. Since, $\Delta < \Delta_c$ no hardening effect was observed for $E/S_Y = 20$ due to an elastic nature. A significant amount of hardening effect was observed for higher E/S_Y and higher Δ value.

A parametric study was also performed to calculate the surface separation for both the types of hardening and the results were then curve fitted. By normalizing the contact area and average pressure, the current model provides analytical expressions of contact area as a function of the average pressure for the elastic-plastic regime. The errors in the numerical fits are fairly low (less than 5%) and suggest that the fits are reasonable.

References

[1] Westergaard, H. M., 1939, "Bearing Pressures and Cracks," ASME J. Appl. Mech., 6), pp. 49-53.

[2] Ciavarella, M., Demelio, G., Barber, J. R., and Jang, Y. H., 2000, "Linear Elastic Contact of the Weierstrass Profile," Proceedings of the Royal Society of London. Series A: Mathematical, Physical and Engineering Sciences, 456(1994), pp. 387-405.

[3] Gao, Y. F., Bower, A. F., Kim, K. S., Lev, L., and Cheng, Y. T., 2006, "The Behavior of an Elastic–Perfectly Plastic Sinusoidal Surface under Contact Loading," Wear, 261(2), pp. 145-154.

[4] Krithivasan, V., and Jackson, R. L., 2007, "An Analysis of Three-Dimensional Elasto-Plastic Sinusoidal Contact," Tribology Letters, 27(1), pp. 31-43.

[5] Jackson, R. L., Krithivasan, V., and Wilson, W. E., 2008, "The Pressure to Cause Complete Contact between Elastic—Plastic Sinusoidal Surfaces," Proceedings of the Institution of Mechanical Engineers, Part J: Journal of Engineering Tribology, 222(7), pp. 857-863.

[6] Gao, Y. F., Bower, A. F., Kim, K. S., Lev, L., and Cheng, Y. T., 2006, "The Behavior of an Elastic–Perfectly Plastic Sinusoidal Surface under Contact Loading," Wear, 261(2), pp. 145-154.

[7] Krithivasan, V., and Jackson, R. L., 2007, "An Analysis of Three-Dimensional Elasto-Plastic Sinusoidal Contact," Tribology Letters, 27(1), pp. 31-43.

[8] Tabor, D., 1951, "The Hardness of Materials," Claredon Press, Oxford, UK, 131(pp. 357-364.

[9] Greenwood, J. A., and Williamson, J. B. P., 1966, "Contact of Nominally Flat Surfaces,"

Proceedings of the Royal Society of London. Series A. Mathematical and Physical Sciences, 295(1442), pp. 300-319.

[10] Archard, J., 1957, "Elastic Deformation and the Laws of Friction," Proceedings of the Royal Society of London. Series A. Mathematical and Physical Sciences, 243(1233), pp. 190-205.

[11] Chang, W. R., Etsion, I., and Bogy, D. B., 1987, "An Elastic-Plastic Model for the Contact of Rough Surfaces," Journal of Tribology, 109(2), pp. 257-263.

[12] Jackson, R. L., and Kogut, L., 2006, "A Comparison of Flattening and Indentation Approaches for Contact Mechanics Modeling of Single Asperity Contacts," Journal of Tribology, 128(1), pp. 209- 212.

[13] Polycarpou, A. A., and Etsion, I., 1999, "Analytical Approximations in Modeling Contacting Rough Surfaces," Journal of Tribology, 121(2), pp. 234-239.

[14] Kogut, L., and Etsion, I., 2002, "Elastic-Plastic Contact Analysis of a Sphere and a Rigid Flat," Journal of Applied Mechanics, 69(5), pp. 657-662.

[15] Jackson, R. L., and Green, I., 2005, "A Finite Element Study of Elasto-Plastic Hemispherical Contact against a Rigid Flat," Transactions of the ASME-F-Journal of Tribology, 127(2), pp. 343- 354.

[16] Lin, L. P., and Lin, J. F., 2005, "An Elastoplastic Microasperity Contact Model for Metallic Materials," Journal of Tribology, 127(3), pp. 666-672.

[17] Lévesque, F., Goudreau, S., and Cloutier, L., 2011, "Elastic-Plastic Microcontact Model for Elliptical Contact Areas and Its Application to a Treillis Point in Overhead Electrical Conductors," Journal of Tribology, 133(1), pp.

[18] 林黎柏, and 林仁輝, 2009, "Effects of Ellipticity of Contact Area and Poisson's Ratio on

the Yielding Behavior of Two Contact Solids," pp.

[19] Jamari, J., and Schipper, D., 2006, "An Elastic–Plastic Contact Model of Ellipsoid Bodies," Tribology Letters, 21(3), pp. 262-271.

[20] Johnson, K.L., Greenwood, J.A, and Higginson, J.G., *The contact of elastic regular wavy surfaces.*, Int.J.Mech.Sci., 1985. 27(6): p. 383-396.

[21] Westergaard, H. M., 1939, "Bearing Pressures and Cracks," ASME J. Appl. Mech., 6), pp. 49-53.

[22] Ciavarella, M., Demelio, G., Barber, J. R., and Jang, Y. H., 2000, "Linear Elastic Contact of the Weierstrass Profile," Proceedings of the Royal Society of London. Series A: Mathematical, Physical and Engineering Sciences, 456(1994), pp. 387-405.

[23] Gao, Y. F., Bower, A. F., Kim, K. S., Lev, L., and Cheng, Y. T., 2006, "The Behavior of an Elastic–Perfectly Plastic Sinusoidal Surface under Contact Loading," Wear, 261(2), pp. 145-154.

[24] Krithivasan, V., and Jackson, R. L., 2007, "An Analysis of Three-Dimensional Elasto-Plastic Sinusoidal Contact," Tribology Letters, 27(1), pp. 31-43.

[25] Jackson, R. L., Krithivasan, V., and Wilson, W. E., 2008, "The Pressure to Cause Complete Contact between Elastic—Plastic Sinusoidal Surfaces," Proceedings of the Institution of Mechanical Engineers, Part J: Journal of Engineering Tribology, 222(7), pp. 857-863.

[26] Johnson, K. L., Greenwood, J. A., and Higginson, J. G., 1985, "The Contact of Elastic Regular Wavy Surfaces," International Journal of Mechanical Sciences, 27(6), pp. 383-396.

[27] Jackson, R. L., and Streator, J. L., 2006, "A Multi-Scale Model for Contact between Rough Surfaces," Wear, 261(11), pp. 1337-1347.

[28] Jackson, R. L., and Green, I., 2005, "A Finite Element Study of Elasto-Plastic

Hemispherical Contact against a Rigid Flat," Transactions of the ASME-F-Journal of Tribology, 127(2), pp. 343- 354.

[29] Greenwood, J.A. and Williamson, J.B.P, *Contact of nominally flat surfaces.*, Proc.R. Soc. Lond., 1966. A(295): p. 300-319.

[30] Majumdar, A., and Tien, C. L., *Fractal characterization and simulation of rough surfaces*, Wear, 1990. 136: p. 313-327.

[31] Kogut, L., and Jackson, R. L., *A comparison of contact modeling utilizing statis- tical and fractal approaches*, ASME J. Tribol., 2006. 128: p. 213-217.

[32] Majumdar, A. and B. Bhushan (1991). "Fractal Model of Elastic-Plastic Contact between Rough Surfaces." Journal of Tribology-Transactions of the Asme **113**(1): 1-11.

[33] Saha, Swarna, and Jackson, "Elasic plastic axisymmetric sinusoidal surface asperity contact", electrical contacts (Holm), 2016 IEEE.

[34] L.Kogut and I.Etsion, "Elastic-Plastic contact analysis of a sphere and rigid flat.", ASME J. Tribol., 2002, 657-662.

ANSYS Simulation Code (Power Law Hardening)

```
/PREP7

!---------------------------------DEFINING CONSTANTS--------------------------------------

*SET, N, 100                 ! NUMBER OF NODES IN X AND Y DIRECTIONS
*SET, HALF_LAMBDA, 0.5
*SET,AMPLITUDE, 0.005
*SET, PI, 3.1415926
*SET, N_HARDENING, 0.45       ! HARDENING EXPONENT IN THE POWER LAW
ISOTROPIC HARDENING
*SET, DELTA_X, (HALF_LAMBDA)/(N) ! INTERVALS BETWEEN THE NEIGHBORING
KEY POINTS [MM]
*SET,HEIGHT,-1.2


!---------------------------------ELEMENT-----------------------------------------------

ET,1,PLANE183
KEYOPT,1,1,0
KEYOPT,1,3,1
KEYOPT,1,6,0


!--------------------------------------Create contact pair---------------------------------------
MP,MU,1,0
R,3
REAL,3

ET,2,169
ET,3,172
R,3,,,1.0,0.01,
KEYOPT,3,2,0
KEYOPT,3,3,1
KEYOPT,3,5,1
KEYOPT,3,10,2
KEYOPT,3,12,0


!-----------------------------------MATERIAL PROPERTIES------------------------------------
```

```
MP, EX, 1, 200E3      ! ELASTIC MODULUS [N/(mm^2)]
MP, PRXY, 1, 0.33     ! POISSON'S RATIO
TB, NLISO, 1,,, POWER     ! NONLINEAR POWER LAW ISOTROPIC HARDENING
TBDATA,,100,0.45      ! Yield strength and hardening exponent
!-----------------------------------GEOMETRY-------------------------------------------------

*DIM, XX, ARRAY, N+1        ! COORDINATE OF THE KEYPOINTS IN X DIRECTION
*DIM, YY, ARRAY, N+1        ! HEIGHT OF THE KYPOINTS ON THE SINUSOIDAL CURVE

*DO, I, 1, N+1            !NODAL COORDINATE IN THE X DIRECTION [mm]
*SET, XX(I), DELTA_X*(I - 1)
*ENDDO

*DO, I, 1, N+1                !NODAL COORDINATE ALONG THE SINUSOIDAL SURFACE
[mm]
*SET, YY(I), AMPLITUDE+AMPLITUDE*cos(2*PI*XX(I))
*ENDDO

*DO, I, 1, N+1        ! CREATING THE KEY POINTS ALONG X DIRECTION
K, I, XX(I), YY(I), 0
*ENDDO

*DO,I,1,10
L,I,I+1
*ENDDO

CM, Sinusoidala, LINE          ! CREATE A LINE COMPONENT CONSISTS OF ALL THE
SUB-LINES IN THE SINUSOIDAL PROFILE

K,N+2,0,YY(1)-XX(11),0
LARC,11,102,1,XX(11)

L,1,N+2

LSEL, S, LOC, Y, (YY(1)-XX(11))- 1e-10 ,YY(1)+1e-10
AL,ALL

LSEL,U,LINE,,ALL

*DO,I,N-9,N
L,I,I+1
*ENDDO

CM, Sinusoidalb, LINE          ! CREATE A LINE COMPONENT CONSISTS OF ALL THE
SUB-LINES IN THE SINUSOIDAL PROFILE
```

```
K,N+3,XX(N+1),-XX(11),0
LARC,91,103,101,XX(11)

L,N+3,N+1

AL,ALL

LSEL,U,LINE,,ALL

*DO, I, 11, N-10          ! CONNECTING THE NEIGHBORING KEY POINTS (I AND I + 1)
ALONG X AXIS TO FORM THE
L, I, I + 1
*ENDDO

CM, Sinusoidalc, LINE          ! CREATE A LINE COMPONENT CONSISTS OF ALL THE
SUB-LINES IN THE SINUSOIDAL PROFILE

K,N+4,0,HEIGHT*0.15,0
K,N+5,XX(N+1),HEIGHT*0.15,0

L,N+2,N+4
L,N+4,N+5
L,N+5,N+3

LSEL,A,LINE,,11
LSEL,A,LINE,,23
AL,ALL
ALLSEL
AGLUE,1,3
AGLUE,2,3
k , N+6 , HALF_LAMBDA , HEIGHT*0.6 , 0
k , N+7 , 0 , HEIGHT*0.6 , 0
L, N+4, N+7
L, N+7, N+6
L, N+6, N+5
LSEL, S, LOC, Y, HEIGHT*0.6-1e-10, HEIGHT*0.15+ 1e-10
AL,ALL
ALLSEL
K , N+8 , HALF_LAMBDA , HEIGHT , 0
k , N+9 , 0 , HEIGHT , 0
L,N+7, N+9
L,N+9, N+8
L,N+8, N+6
LSEL, S, LOC, Y, HEIGHT-1e-10, HEIGHT*0.6+ 1e-10
AL,ALL
ALLSEL
```

```
AGLUE,3,4
AGLUE,4,5
ALLSEL
K,N+10, XX(1),YY(1),0
K,N+11, XX(N+1),YY(1),0
L,N+10,N+11
ALLSEL


!---------------------------------Meshing-------------------------------------------------------------------

*DO, I ,1, 10
LESIZE, I,,,10,1
*ENDDO
LESIZE, 11,,,100,1
LESIZE, 12,,,100,1
type,1
mat,1
secn,1          !use general axisymmetric section
amesh,1          !generate the master plane
eplot            !visualise the 2D model
ALLSEL
*DO, I ,13, 22
LESIZE, I,,,10,1
*ENDDO
LESIZE, 24,,,100,1
LESIZE, 23,,,100,1
type,1
mat,1
secn,1           !use general axisymmetric section
amesh,2          !generate the master plane
eplot            !visualise the 2D model
ALLSEL
*DO, I ,25, 104
LESIZE, I,,,10,1
*ENDDO
ESIZE,0.004
type,1
mat,1
secn,1           !use general axisymmetric section
amesh,3          !generate the master plane
eplot            !visualise the 2D model
ALLSEL
ESIZE,0.006
type,1
mat,1
secn,1           !use general axisymmetric section
```

```
amesh,4          !generate the master plane
eplot            !visualise the 2D model
ALLSEL
ESIZE,0.007
type,1
mat,1
secn,1           !use general axisymmetric section
amesh,5          !generate the master plane
eplot            !visualise the 2D model
ALLSEL
TYPE,2
LMESH,114        !generate the master plane
eplot            !visualise the 2D model
ALLSEL


!-------------------------- GENERATE CONTACT SURFACE-------------------------------------------
--!

CMSEL, S, Sinusoidala, LINE
CMSEL, A, Sinusoidalb, LINE
CMSEL, A, Sinusoidalc, LINE
TYPE,3
NSLL, S, 1                    ! SELECT ALL NODES ASSOCIATED WITH THE SINUSOIDAL
PROFILE
ESLN, S, 0           ! SELECT ELEMENTS ASSOCIATED WITH THE SELECTED NODES
ESURF
ALLSEL
TYPE, 2
TSHAP, PILO
*GET,NODE_NO,NODE,0,NUM,MAX
N, NODE_NO+1 ,XX(1), YY(1), 0
E, NODE_NO+1
NSEL, S , , , NODE_NO+1! SELECT THE NEWLY CREATED NODE
CM, PILOT, NODE
ALLSEL


!---------------------------BOUNDARY CONDITIONS----------------------------------------------------!

LSEL, S, LOC, X, 0-1e-10, 0+ 1e-10
DL, ALL, , UX, 0
ALLSEL
LSEL, S, LOC, X, HALF_LAMBDA-1e-10, HALF_LAMBDA+ 1e-10
DL, ALL, , UX, 0
ALLSEL
LSEL, S, LOC, Y, HEIGHT-1e-10, HEIGHT+ 1e-10
DL, ALL, , UX, 0
```

```
ALLSEL
LSEL, S, LOC, Y, HEIGHT-1e-10, HEIGHT+ 1e-10
DL, ALL, , UY, 0
ALLSEL


!----------------------------SOLUTION_----------------------------------------------------------------!

D, PILOT, UY,-0.02  ! MOVE PILOT NODE (RIGID FLAT) ALONG 0I + 0J +PENE K
D, PILOT, UX, 0
D, PILOT, ROTZ, 0 ! NO ROTATION
/SOL
ANTYPE, 0               ! STATIC ANSLYSI
NLGEOM, ON                 ! LARGE (NONLINEAR) DEFLECTION
TIME,1
AUTOTS, ON               ! USER DEFINED TIME STEP
NSUBST, 800,10000,800        ! NUMBER OF SUBSTEPS IN ONE LOADING STAGE
OUTRES,ALL, ALL             ! WRITE ALL SOLUTIONS FOR ALL SUBSTEPS
NEQIT,200,100             ! MAXIMUM 20 ITERATIONS ON EACH SUBSTEP
KBC, 0                ! USING RAMPED LOAD
BCSOPTION,,INCORE,,,
SOLVE
SAVE



!----------------------------------POST PROCESSING--------------------------------------------------------!

/POST1
ALLSEL
 LSEL, S, LOC, Y, HEIGHT-1e-10, HEIGHT+ 1e-10
NSLL,S,1
*GET, NUM_NODE, NODE, 0, COUNT
 ! INITIALIZE AN ARRAY WHICH IS USED TO STORE THE NUMBER OF EACH
CONTA172 ELEMENT
*DIM, NODE_INDEX , ARRAY, NUM_NODE
*VGET, NODE_INDEX, NODE, , NLIST
ALLSEL
*SET, NUM_CONT_ELEM, 0
 ESEL, S, TYPE, , 3         ! SELECT ELEMENT ATTACHED TO CONTA172
NSLE, S, ALL                ! SELECT ALL THE NODES CONTAINED IN CONTA172
ELEMENT
! OBTAIN NUMBER OF CONTA172 ELEMENTS
*GET, NUM_CONT_ELEM, ELEM, 0, COUNT
! INITIALIZE AN ARRAY WHICH IS USED TO STORE THE NUMBER OF EACH
CONTA172 ELEMENT
*DIM,  CONT_ELEM_NUM , ARRAY, NUM_CONT_ELEM
*DIM,  CONT_ELEM_LOC , ARRAY, NUM_CONT_ELEM
```

```
*VGET, CONT_ELEM_NUM, ELEM, , ELIST
ALLSEL
 *DO,I,1,NUM_CONT_ELEM
*GET,CONT_ELEM_LOC(I),ELEM,CONT_ELEM_NUM(I),CENT,X
*ENDDO
 *DIM,  CONT_ELEM_NUM_SORTED , ARRAY, NUM_CONT_ELEM
*DIM,  CONT_ELEM_LOC_SORTED , ARRAY, NUM_CONT_ELEM

*DO,I,1,NUM_CONT_ELEM
*SET,CONT_ELEM_NUM_SORTED(I),CONT_ELEM_NUM(I)
*ENDDO
*DO,I,1,NUM_CONT_ELEM
*SET,CONT_ELEM_LOC_SORTED(I),CONT_ELEM_LOC(I)
*ENDDO
*DO,p,1,NUM_CONT_ELEM-1
*DO,I,p, NUM_CONT_ELEM-1
*IF, CONT_ELEM_LOC_SORTED(p) , GT , CONT_ELEM_LOC_SORTED(I+1), THEN
*SET,TEMP_SINE,CONT_ELEM_LOC_SORTED(I+1)
*SET,CONT_ELEM_LOC_SORTED(I+1),CONT_ELEM_LOC_SORTED(p)
*SET,CONT_ELEM_LOC_SORTED(p),TEMP_SINE
*SET,TEMP_SINE,CONT_ELEM_NUM_SORTED(I+1)
*SET,CONT_ELEM_NUM_SORTED(I+1),CONT_ELEM_NUM_SORTED(p)
*SET,CONT_ELEM_NUM_SORTED(p),TEMP_SINE
*ENDIF
 *ENDDO
*ENDDO
*DO,p,2,NUM_CONT_ELEM-1
*DO,I,p, NUM_CONT_ELEM-1
*IF, CONT_ELEM_LOC_SORTED(p) , GT , CONT_ELEM_LOC_SORTED(I+1), THEN
*SET,TEMP_SINE,CONT_ELEM_LOC_SORTED(I+1)
*SET,CONT_ELEM_LOC_SORTED(I+1),CONT_ELEM_LOC_SORTED(p)
*SET,CONT_ELEM_LOC_SORTED(p),TEMP_SINE
*SET,TEMP_SINE,CONT_ELEM_NUM_SORTED(I+1)
*SET,CONT_ELEM_NUM_SORTED(I+1),CONT_ELEM_NUM_SORTED(p)
*SET,CONT_ELEM_NUM_SORTED(p),TEMP_SINE
*ENDIF
*ENDDO
*ENDDO
*GET,NOSUB,ACTIVE,0,SOLU,NCMSS
*DIM,CONT_ELEM_STAT,ARRAY,NUM_CONT_ELEM+1
*DIM,CONTACT_AREA,ARRAY,NOSUB
*DIM,REACTION_FORCE,ARRAY,NOSUB
*DO,I,1,NOSUB
*GET,N_O_COLUMN,ETAB,0,NCOL,MAX
*IF,N_O_COLUMN,GT,0,THEN
ETABLE,ERASE
```

```
*ENDIF
 SUBSET, 1,I            ! VISIT EACH SUB-LOADING STEP OF THE 1ST LOADING STEP
ESEL, S, TYPE, , 3        ! SELECT ELEMENT ATTACHED TO CONTA172
NSLE, S, ALL              ! SELECT ALL THE NODES CONTAINED IN CONTA172
ELEMENT
ETABLE,CONSTAT1,NMISC,2
ETABLE,CONSTAT2,NMISC,1
ETABLE,CONSTAT3,NMISC,19
*SET,FORCE,0
*GET,CONT_ELEM_STAT(1),ETAB,1,ELEM,CONT_ELEM_NUM_SORTED(1)
*DO,J,2,NUM_CONT_ELEM+1
*GET,CONT_ELEM_STAT(J),ETAB,2,ELEM,CONT_ELEM_NUM_SORTED(J-1)
*ENDDO
*SET,COUNT,NUM_CONT_ELEM
*DO, J,1,NUM_CONT_ELEM+1

*IF,COUNT,LT,3,THEN
*SET,COUNT,1
*ENDIF
*GET,NODE_NO,ELEM,CONT_ELEM_NUM_SORTED(COUNT),NODE,1
*GET,X_COR,NODE,NODE_NO,LOC,X
 *IF,CONT_ELEM_STAT(COUNT+1),EQ,2,EXIT
 *SET,COUNT,COUNT-1
*ENDDO
*IF,X_COR,LT,XX(N+1),THEN
*IF,CONT_ELEM_STAT(COUNT+1),EQ,2,THEN
*GET,a,ETAB,3,ELEM,CONT_ELEM_NUM_SORTED(COUNT+1)
*IF,a,NE,2,THEN
*GET,NODE_NO,ELEM,CONT_ELEM_NUM_SORTED(COUNT+1),NODE,2
*GET,X_COR,NODE,NODE_NO,LOC,X
*GET,X_DEF,NODE,NODE_NO,U,X
*SET,CONTACT_AREA(I),PI*(X_COR+X_DEF)**2
*ELSE
*GET,NODE_NO1,ELEM,CONT_ELEM_NUM_SORTED(COUNT+1),NODE,2
*GET,X_COR1,NODE,NODE_NO1,LOC,X
*GET,X_DEF1,NODE,NODE_NO1,U,X
*GET,NODE_NO2,ELEM,CONT_ELEM_NUM_SORTED(COUNT+1),NODE,1
*GET,X_COR2,NODE,NODE_NO2,LOC,X
*GET,X_DEF2,NODE,NODE_NO2,U,X
*SET,RAD,(X_COR1+X_DEF1+X_COR2+X_DEF2)/2
*SET,CONTACT_AREA(I),PI*(RAD**2)
*ENDIF

*ENDIF
*ELSE
*GET,X_DEF,NODE,NODE_NO,U,X
```

```
*SET,CONTACT_AREA(I),PI*(X_COR+X_DEF)**2
*ENDIF
ALLSEL
*DO,P,1,NUM_NODE
*GET,FORCE_1,NODE,NODE_INDEX(P),RF,FY
*SET,FORCE,FORCE+FORCE_1
*SET,FORCE_1,FORCE
*ENDDO
*SET,REACTION_FORCE(I),FORCE_1
*ENDDO
/INPUT, WRITE, txt
```

Appendix B

ANSYS Simulation code for surface separation

```
/POST1
 ALLSEL
 *SET, NUM_CONT_ELEM, 0
ESEL, S, TYPE, , 3          ! SELECT ELEMENT ATTACHED TO CONTA172
NSLE, S, ALL               ! SELECT ALL THE NODES CONTAINED IN CONTA172
ELEMENT

! OBTAIN NUMBER OF CONTA172 ELEMENTS
*GET, NUM_CONT_ELEM, ELEM, 0, COUNT     !Determining total number of contact
element
! INITIALIZE AN ARRAY WHICH IS USED TO STORE THE NUMBER OF EACH
CONTA172 ELEMENT
*DIM,  CONT_ELEM_NUM , ARRAY, NUM_CONT_ELEM
*DIM,  CONT_ELEM_LOC , ARRAY, NUM_CONT_ELEM
*VGET, CONT_ELEM_NUM, ELEM, , ELIST      ! Determining the number of each contact
element(Serial doesn't match geometry serial no of contact element)
ALLSEL
*DO,I,1,NUM_CONT_ELEM
*GET,CONT_ELEM_LOC(I),ELEM,CONT_ELEM_NUM(I),CENT,X  ! Determining the mid
location of each contact element
*ENDDO
!************************** Sorting the contact elent baSED ON the mid location of
contact element so that serial match geomtry serial*************
 *DIM,  CONT_ELEM_NUM_SORTED , ARRAY, NUM_CONT_ELEM
*DIM,  CONT_ELEM_LOC_SORTED , ARRAY, NUM_CONT_ELEM
*DO,I,1,NUM_CONT_ELEM
*SET,CONT_ELEM_NUM_SORTED(I),CONT_ELEM_NUM(I)
*ENDDO
 *DO,I,1,NUM_CONT_ELEM
*SET,CONT_ELEM_LOC_SORTED(I),CONT_ELEM_LOC(I)
*ENDDO
 *DO,p,1,NUM_CONT_ELEM-1
*DO,I,p, NUM_CONT_ELEM-1
*IF, CONT_ELEM_LOC_SORTED(p) , GT , CONT_ELEM_LOC_SORTED(I+1), THEN
*SET,TEMP_SINE,CONT_ELEM_LOC_SORTED(I+1)
*SET,CONT_ELEM_LOC_SORTED(I+1),CONT_ELEM_LOC_SORTED(p)
*SET,CONT_ELEM_LOC_SORTED(p),TEMP_SINE
```

```
*SET,TEMP_SINE,CONT_ELEM_NUM_SORTED(I+1)
*SET,CONT_ELEM_NUM_SORTED(I+1),CONT_ELEM_NUM_SORTED(p)
*SET,CONT_ELEM_NUM_SORTED(p),TEMP_SINE
 *ENDIF
 *ENDDO
*ENDDO
 *DO,p,2,NUM_CONT_ELEM-1
*DO,I,p, NUM_CONT_ELEM-1
*IF, CONT_ELEM_LOC_SORTED(p) , GT , CONT_ELEM_LOC_SORTED(I+1), THEN
*SET,TEMP_SINE,CONT_ELEM_LOC_SORTED(I+1)
*SET,CONT_ELEM_LOC_SORTED(I+1),CONT_ELEM_LOC_SORTED(p)
*SET,CONT_ELEM_LOC_SORTED(p),TEMP_SINE
*SET,TEMP_SINE,CONT_ELEM_NUM_SORTED(I+1)
*SET,CONT_ELEM_NUM_SORTED(I+1),CONT_ELEM_NUM_SORTED(p)
*SET,CONT_ELEM_NUM_SORTED(p),TEMP_SINE
 *ENDIF
  *ENDDO
*ENDDO
```

!**************************************End of
sorting***

```
*GET,NOSUB,ACTIVE,0,SOLU,NCMSS          ! Get total no. of substep
```

!*******************************Defining array and other
constants**************************************

```
*DIM,R1,ARRAY,NUM_CONT_ELEM              ! Location+deformation of the left node of the
contact element
*DIM,R2,ARRAY,NUM_CONT_ELEM              ! Location+deformation of the right node of
the contact element
*DIM,Y1,ARRAY,NOSUB                      ! Location+deformation of pilot node
*DIM,Y2,ARRAY,NUM_CONT_ELEM+1           ! Location+deformation of the each node of
the contact element
*DIM,RADIUS,ARRAY,NUM_CONT_ELEM+1        ! x LOCATION +deformation OF each
node on sinusoidal surface
*DIM,DISTANCE,ARRAy,NUM_CONT_ELEM+1      ! GAP between rigid flat and sinusoidal
asperity
*DIM,CONT_ELEM_STAT,ARRAY,NUM_CONT_ELEM+1 ! Contact element status of each
node at the contact
*DIM,AVG_GAP,ARRAY,NOSUB                 ! Average gap during each substep
ALLSEL
LSEL,S,LINE,,114
NSLL,S,1
```

!*****************GET pilot node location for each
substep**

```
*DO,I,1,578
SUBSET, 1,I              ! VISIT EACH SUB-LOADING STEP OF THE 1ST LOADING
STEP
```

```
*GET,Y_COR,NODE,221847,LOC,Y     ! pilot node location ******CHANGE************
*SET,Y_DEF,UY(221847)            ! Pilot node deformation****CHANGE************
*SET,Y1(I),Y_COR+Y_DEF
*ENDDO
ALLSEL
!*****************Determining the location of each node on the sinusoidal
asperity**********************
*DO,I,1,578
SUBSET, 1,I
  ESEL, S, TYPE, , 3                            ! SELECT ELEMENT ATTACHED TO
CONTA172
NSLE, S, ALL
ETABLE,CONSTAT1,NMISC,2                    ! status of the nodes of each contact
element
ETABLE,CONSTAT2,NMISC,1
*GET,NODE_NO,ELEM,CONT_ELEM_NUM_SORTED(1),NODE,2   ! Determining the y co-
ordinate of the nodes on the sinusoidal surface before division
*GET,Y_COR1,NODE,NODE_NO,LOC,Y
*GET,Y_DEF1,NODE,NODE_NO,U,Y
*SET,Y2(1),Y_COR1+Y_DEF1
*DO,J,1,NUM_CONT_ELEM
*GET,NODE_NO,ELEM,CONT_ELEM_NUM_SORTED(J),NODE,1
*GET,Y_COR1,NODE,NODE_NO,LOC,Y
*GET,Y_DEF1,NODE,NODE_NO,U,Y
*SET,Y2(J+1),Y_COR1+Y_DEF1
*ENDDO
*DO,J,1,NUM_CONT_ELEM                              ! Determining the x co-ordinate of
the nodes on the sinusoidal surface before division
*GET,NODE_NO1,ELEM,CONT_ELEM_NUM_SORTED(J),NODE,2
*GET,X_COR1,NODE,NODE_NO1,LOC,X
*GET,X_DEF1,NODE,NODE_NO1,U,X
*SET,R1(J),X_COR1+X_DEF1
*GET,NODE_NO2,ELEM,CONT_ELEM_NUM_SORTED(J),NODE,1
*GET,X_COR2,NODE,NODE_NO2,LOC,X
*GET,X_DEF2,NODE,NODE_NO2,U,X
*SET,R2(J), X_COR2+X_DEF2
*ENDDO
*SET,RADIUS(1),R1(1)
*DO,J,1,NUM_CONT_ELEM
*SET,RADIUS(J+1),R2(J)
*ENDDO
*DO,J,1,NUM_CONT_ELEM+1
*SET,a,Y1(I)-Y2(J)
*SET,DISTANCE(J),a                      ! Determining gap between rigid flat and
sinusoidal surface after division
*ENDDO
```

```
!/INPUT,Test,txt
*GET,CONT_ELEM_STAT(1),ETAB,1,ELEM,CONT_ELEM_NUM_SORTED(1)
*DO,J,2,NUM_CONT_ELEM+1
*GET,CONT_ELEM_STAT(J),ETAB,2,ELEM,CONT_ELEM_NUM_SORTED(J-1)
*ENDDO
*DO,J,NUM_CONT_ELEM+1,1,-1
*IF,CONT_ELEM_STAT(J),EQ,2,EXIT
*ENDDO
*SET,LAST_NODE_IN_CONTACT,J
*SET,RAD1,RADIUS(LAST_NODE_IN_CONTACT)
*Do,J,1,LAST_NODE_IN_CONTACT                          ! Making the gap zero from the first
to the last node in contact
*SET,DISTANCE(J),0
*ENDDO
*DO,J,LAST_NODE_IN_CONTACT,NUM_CONT_ELEM+1      ! where there is gap, if there
is any penetration make that node gap zero
*IF,DISTANCE(J),LT,0,THEN
*SET,DISTANCE(J),0
*ENDIF
*ENDDO
!/INPUT,Test,txt
! *****************End of the part that has done to avoid numerical
error******************************************
!*****************CAlculation of volume of gap and area of
gap*********************************************************
*SET,RAD2,RADIUS(NUM_CONT_ELEM+1)
*SET,VOLUME,0
*IF,LAST_NODE_IN_CONTACT,EQ,NUM_CONT_ELEM+1,THEN
*SET,VOLUME,0
*SET,RAD1,0

*ELSE
*DO,P,LAST_NODE_IN_CONTACT+1,NUM_CONT_ELEM+1
*SET,VOLUME,VOLUME+(2*PI*RADIUS(P)*DISTANCE(P)+2*PI*RADIUS(P-
1)*DISTANCE(P-1))*(RADIUS(P)-RADIUS(P-1))/2                ! Trapezoidal rule has been
applied to calculate gap volume
*ENDDO
*ENDIF
*SET,AVG_GAP(I),VOLUME/(PI*((RAD2)**2-(RAD1)**2))
                                ! Calculating average gap
*ENDDO
/INPUT,WRITE1,txt
```

Appendix C

Post Processing files for Appendix A and Appendix B

Post Processing File for Appendix A
*MWRITE, CONTACT_AREA, CONTACT_AREA, txt, , IJK, NOSUB
(E30.20)
*MWRITE, REACTION_FORCE, REACTION_FORCE, txt, , IJK, NOSUB
(E30.20)

Post Processing File for Appendix B
*MWRITE, AVG_GAP, AVG_GAP, txt, , IJK, NOSUB
(E30.20)